Signalling from mTOR to eIF2α mediates cell migration in response to the chemotherapeutic doxorubicin

Robert F. Harvey, Tuija A. A. Pöyry, Mark Stoneley and Anne E. Willis*

Medical Research Council Toxicology Unit, University of Cambridge, Lancaster Rd, Leicester LE1 9HN UK.

* Correspondence: aew80@mrc-tox.cam.ac.uk

One Sentence Summary

Crosstalk signalling from mTOR to eIF2 in response to the chemotherapeutic doxorubicin mediates cell migration

Abstract

Following exposure to cytotoxic chemotherapeutics, tumour cells alter their translatome to promote cell survival programmes through the regulation of eukaryotic initiation factor (eIF) 4F and ternary complex. Compounds that block mTOR signalling to eIF4F complex formation, such as rapamycin and its analogues, have been used in combination therapies to enhance cell killing, although their success has been rather limited. This is likely to result from the fact that the crosstalk between signalling pathways which co-ordinate eIF4F regulation with ternary complex formation following treatment with genotoxic therapeutics has not been fully explored. Herein, we describe a regulatory pathway downstream of p53 whereby inhibition of mTOR, following DNA damage, promotes crosstalk signalling and leads to eIF2α phosphorylation. We show that eIF2α phosphorylation does not inhibit protein synthesis, but is instead required for cell migration. Importantly, blocking this pathway by chemical intervention with either ISRIB or Trazadone limits cell migration, supporting the notion that therapeutic targeting of eIF2α signalling could restrict tumour cell metastasis and invasion and would be beneficial to subsets of cancer patients.

Introduction

Protein synthesis is one of the most energy-consuming cellular metabolic processes (*1*), and in response to stress or damage, mammalian cells rapidly reprogram protein synthesis to reduce energy demands and adapt to the stress imposed (*2*). Control of protein synthesis is complex, with many regulatory signalling pathways converging on the factors regulating cap-dependent mRNA translation, which is a three step process (initiation, elongation and termination). The process of mRNA translation is predominantly regulated through the modification of the phosphorylation status of eukaryotic initiation (eIF) and elongation (eEF) factors (*3*).

Regulation of protein synthesis at initiation is controlled by two critical rate-limiting steps; eIF4F assembly and ternary complex (TC) formation (*3*). The eIF4F complex (comprised of the cap-binding protein eIF4E, the DEAD-box helicase eIF4A, and the scaffold protein eIF4G) assembles at the 5' cap structure of mRNA. eIF4E bioavailability, and thus eIF4F complex formation, is regulated by a family of eIF4E-binding proteins (4E-BPs) that compete with eIF4G for a single binding site on eIF4E (*4*). Through this mechanism, 4E-BPs inhibit cap-dependent translation by preventing the subsequent recruitment of the 43S complex. The capacity of 4E-BPs to bind eIF4E is regulated by mechanistic target of rapamycin complex 1 (mTORC1). In response to growth factors and amino acids, mTORC1 positively regulates translation initiation through the phosphorylation of 4E-BPs and p70 S6K (*5*). Upon mTORC1 activation, 4E-BPs are hyper-phosphorylated, inhibiting binding to eIF4E and thereby enabling eIF4F formation. Conversely, in response to mTORC1 inhibition, 4E-BPs are hypo-phosphorylated, promoting their binding to eIF4E and inhibition of eIF4F formation (*6*).

The TC is comprised of eIF2 in complex with GTP and the initiator tRNA ($tRNAi^{met}$), and functions to deliver this tRNA to the 43S complex during translation initiation. After start codon recognition, eIF2 undergoes GTP hydrolysis and is released from the initiation complex as eIF2-GDP, which is then recycled by the guanine nucleotide exchange factor (GEF) eIF2B

back to eIF2-GTP (*3*). eIF2 is phosphorylated within the α subunit (eIF2α) in response to a range of stresses, which enhances the affinity of eIF2-GDP for eIF2B, thus decreasing the availability of TC and inhibiting translation initiation (*7*). Four eIF2 kinases (eIF2Ks) have been identified in mammalian cells: GCN2 (general control non-derepressible-2), PKR (protein kinase double-stranded RNA-dependent), PERK (PKR-like ER kinase), and HRI (hemeregulated inhibitor), which phosphorylate eIF2α in response to a range of stress stimuli including amino acid deprivation, UV-induced DNA damage, viral infection, endoplasmic reticulum (ER) stress and heme deficiency (*8*). In addition to inhibiting global protein synthesis, eIF2α phosphorylation enables the cell to reprogram translation (*2*) and selectively translate mRNAs containing upstream open reading frames (uORFs) (*7*), which encode proteins required for the stress response. For example, in response to bulky DNA adducts-inducing agents, including anti-cancer chemotherapeutics such as cisplatin, protein synthesis is rapidly inhibited via GCN2-dependent phosphorylation of eIF2α (*9*–*11*), while the translation of uORF-containing mRNAs which encode proteins that regulate DNA-damage repair pathways is simultaneously enhanced (*10*, *11*).

The formation of TC and eIF4F were originally thought to be distinct processes that converged to regulate translation initiation. However, it has been shown recently that TC availability and eIF4F formation are exquisitely co-ordinated to provide a robust response to cellular stress. For instance, acute activation of mTORC1 inhibits 4E-BPs and enhances eIF4F formation while simultaneously decreasing eIF2α phosphorylation through a mechanism dependent on the phosphorylation of eIF2β, to increase TC availability (*12*). Conversely, catalytic mTORC1 inhibition has been shown to enhance eIF2α phosphorylation via the PP6c-dependent activation of GCN2 (*13*). Furthermore, PERK/GCN2-dependent eIF2α phosphorylation induced by oxidative stress was shown to diminish mTORC1 activity (*14*), whereas mTORC1 hyper-activation in TSC2 deficient cells diminishes PERK activity and eIF2α phosphorylation (*15*). Moreover, Akt has been implicated in maintaining an inhibitory phosphorylation site on PERK, preventing its activation (*16*). These studies suggest that mTOR- and eIF2K-signalling

are closely intertwined, and enable a cell to form a co-ordinated, specific and robust response to cell stress, as it is not beneficial for a cell to expend energy on forming TC when eIF4F is not present to recruit the 43S subunit.

During tumorigenesis, the same pathways that limit protein synthesis under stressed conditions permit survival and the increased proliferation of cancer cells in the unfavourable growth conditions within the tumour microenvironment. Therefore, the signalling pathways and proteins that are involved in these processes provide attractive therapeutic avenues for cancer treatments (*17–19*). Initially, mTOR inhibitors such as rapamycin and its analogues (rapalogues), including temsirolimus and everolimus, were tested in a wide spectrum of human tumours, as both monotherapies and combination treatments with doxorubicin (Adriamycin) (*20*, *21*), although response rates in clinical trials are modest. More recently, there has been increased research into the consequences of inhibition of signalling from eIF2Ks to restrict activation of the pro-survival unfolded protein response in tumour cells, with some promising data in this regard (*22*, *23*). However, what is poorly understood and has not been investigated is the extent of crosstalk between mTOR- and eIF2K-signalling in response to cancer chemotherapeutics, and how combination therapies based on the inhibition of these pathways impact on cell survival. Here, we set out to address these questions by studying the regulation of protein synthesis in response to doxorubicin-induced DNA damage, and since p53 is pivotal in this response we chose to use the model cell line MCF10A, which is non-tumour derived, and a parallel MCF10A cell line where p53 is deleted (MCF10A$^{p53-/-}$). Importantly, we have identified a novel, DNA-damage specific, crosstalk signalling pathway between mTOR and eIF2 in response to a physiological and clinically relevant stimulus. We show that doxorubicin inhibits protein synthesis via the p53-dependent inhibition of mTOR signalling, and that doxorubicin-induced mTOR inhibition enhances the phosphorylation of eIF2α via the activation of GCN2 and PERK. Moreover, we show that this signalling pathway is functional in a range of cancer cell lines and our data suggest that phosphorylation of eIF2α is not necessary for protein synthesis shut down, but rather under stress conditions it is required for

cell migration, and therefore these data have important implications for the use of inhibitors of these pathways in a clinical setting.

Results

Doxorubicin inhibits global protein synthesis via the mTOR axis

Doxorubicin acts as a topoisomerase II poison at concentrations in excess of 400 nM (*24*, *25*) and at higher doses can generate DNA damage through indirect mechanisms (*25*), including the generation of ROS (*26*). Many studies that use cell culture assays to investigate the mechanism of action of doxorubicin employ concentrations in excess of 1 μM, and although this has provided valuable insights, it should not be considered clinically relevant. Therefore, we chose to study the effects of doxorubicin using a concentration of 500 nM (Fig S1A).

To determine the effect of doxorubicin on global protein synthesis, radiolabelled $^{[35]}$S-methionine incorporation was used. Protein synthesis was not significantly inhibited until 9 hours after treatment with doxorubicin (Fig 1A), a considerable delay from the initial recognition of DNA damage, culminating in a total reduction of over 50% at 24 hours. Sucrose density gradient centrifugation was used to measure the distribution of ribosomes between subpolysomes (free ribosomes) and polyribosomes, and to determine if doxorubicin inhibits ribosome recruitment to mRNA. After treatment with doxorubicin for 6 hours, global protein synthesis was not inhibited (Fig 1A) and this was reflected in the polysome profile analysis, where a minimal decrease in polysomes and increase in subpolysomes was observed (Fig S1B). In contrast, the number of polysomes decreased dramatically when protein synthesis was inhibited at 24 hours, suggesting that the inhibition of initiation blocked ribosome loading onto mRNA (Fig 1B). During a block in translation initiation, ribosomes would ordinarily dissociate from polysomes and accumulate as free ribosomes in subpolysomes. However, ribosomes lost from polysomes did not accumulate within the subpolysomes in response to doxorubicin, suggesting that this treatment does not result in the “classical” initiation block, such as that observed in response to the mTOR inhibitor AZD8055 (Fig S1C). However, these data are consistent with prolonged treatment with doxorubicin resulting in either ribosome

degradation or accumulation of ribosomes within non-soluble stress granules, as has been observed in response to UV-induced DNA damage in yeast (*27*) and mammalian cells (*28*).

mRNA translation initiation is inhibited at the initiation stage by the phosphorylation of 4E-BPs and eIF2, regulating eIF4F and TC formation respectively (Fig 1C). To understand the regulation of eIF2 and 4E-BPs in relation to the inhibition of translation initiation, western blot analysis was used out to determine the cellular signalling response to doxorubicin. The DNA-damage response (DDR) was activated within 3 hours of treatment, as shown by the phosphorylation of ATM and its substrate checkpoint kinase 2 (Chk2) (Fig 1D). Interestingly, eIF2α phosphorylation was not observed until 12 hours after treatment with doxorubicin, at a point when protein synthesis had been robustly inhibited. Moreover, eIF2α phosphorylation was preceded by the inhibition of mTOR signalling, and the dephosphorylation of 4E-BP1 observed at 6-9 hours after treatment (Fig 1D) correlated with the inhibition of protein synthesis.

As eIF2α phosphorylation was only observed after mTORC1 inhibition and did not correlate with the initial inhibition of proteins synthesis, it was important to establish the role played by eIF2α phosphorylation in this regard. To address this question we used the integrated stress response inhibitor (ISRIB), which has been demonstrated to reverse the inhibitory effect of eIF2α phosphorylation on global protein synthesis (*29*). ISRIB does not inhibit the activity of eIF2Ks or the phosphorylation of eIF2α (*29*), but relieves all eIF2α phosphorylation-dependent signalling, such as the induction of ATF-4 expression (*30*). To demonstrate the functionality of ISRIB in MCF10A cells, thapsigargin was used to induce ER stress and inhibit protein synthesis, and this inhibition was reversed by the addition of ISRIB (Fig 1 Ei). However, when MCF10A cells were treated with doxorubicin in the presence of ISRIB, ISRIB did not rescue the reduction in protein synthesis (Fig 1 Eii), indicating that doxorubicin-induced translation inhibition is not dependent on eIF2α phosphorylation. In agreement with previous studies (*30*), immunoblot analysis showed that thapsigargin-induced ATF4 expression was abolished by

co-treatment with ISRIB and thapsigargin-induced eIF2α phosphorylation was unaffected (Fig 1F). However, ISRIB surprisingly abolished doxorubicin-induced eIF2α phosphorylation (Fig 1F), indicating that when cells are subjected to prolonged stress in the presence of ISRIB, the compound may lead to off-target effects or modulate the stress response in an alternative way. Moreover, doxorubicin did not enhance the expression of ATF4 (Fig 1F and S1D) or other proteins that are upregulated during the ISR (Fig 1F). It was somewhat surprising that ATF4 expression was not upregulated in the presence of high levels of eIF2α phosphorylation, however, this was most likely due to a lack of availability of the ATF4 mRNA, as it has been shown previously that ATF4 expression is dependent on the co-ordinated transcriptional and translational regulation during the integrated stress response (ISR) (*31*). Importantly, regardless of the effects of ISRIB on doxorubicin-induced eIF2α phosphorylation, these data strongly suggested that eIF2α phosphorylation did not make a major contribution to doxorubicin-induced inhibition of protein synthesis and instead this was most likely regulated by the inhibition of mTORC1 signalling.

p53 is required for doxorubicin-induced mTORC1 inhibition

p53 is an important mediator of the DDR, arresting the cell cycle to enable to the repair of DNA, or initiating cell death pathways. It has been shown previously that p53 functions as a negative regulator of mTOR signalling (*32*) (Fig 2A) and mTOR activity is enhanced in p53-deficient tumours (*33*). Therefore, we investigated the role of p53 in doxorubicin-induced mTORC1 inhibition using an MCF10A p53 knockout cell line ($p53^{-/-}$).

MCF10A cells with wild-type or deleted p53 ($p53^{+/+}$/$p53^{-/-}$) were treated with doxorubicin or the catalytic mTOR inhibitor AZD8055 for 16 hours, and signalling pathways analysed by western blotting (Fig 2B). As expected, p53 was stabilised and the expression of p53-dependent transcripts such as Sestrin 2 were enhanced in response to doxorubicin in $p53^{+/+}$ cells, whereas these where both abolished in $p53^{-/-}$ cells (Fig 2B). Interestingly, dephosphorylation of p70 S6K induced by doxorubicin was also abolished in $p53^{-/-}$ cells and the reduction of p-

4E-BP1 was modestly relieved (Figs. 2B and 2C). Crucially, catalytic inhibition of mTOR with AZD8055 robustly inhibited mTOR signalling in both $p53^{+/+}$ and $p53^{-/-}$ cell lines (Figs. 2B and 2C), suggesting that p53 may be regulating signalling pathways upstream of mTORC1. This hypothesis was further supported using a siRNA specific to p53 (sip53) to deplete p53 in $p53^{+/+}$ cells. After treatment with doxorubicin, p53-depleted cells lost the reduction of p-p70 S6K that was observed in $p53^{+/+}$ cells transfected with a non-targeting siRNA (Figs. 2D and 2E). However, there was minimal change in the level of p-4E-BP1 (Figs. 2D and 2E), suggesting that an additional signalling mechanism may also regulate 4E-BP1 activity. Tuberous sclerosis complex (TSC) is an important negative regulator of mTORC1 activity (*34*) that has been shown to be activated in response to DNA damage (*35*) (Fig S2A). Importantly, by depleting TSC2 and hence inactivating TSC, our data show that doxorubicin-induced mTORC1 inhibition was independent of TSC (Fig S2B and Fig S2C).

Analysis of polysome profiles, and quantification of the area under the curve of the polysomes and subpolysomes obtained from $p53^{+/+}$ cells treated with doxorubicin, showed a large reduction in polysomally-associated mRNAs (Figs. 1B, 2F and 2G) compared to $p53^{-/-}$ cells (Fig 2G). Moreover, using $^{[35]}$S-methionine incorporation, doxorubicin-induced inhibition of global protein synthesis was also shown to be partially restored after knockout or knockdown of p53 (Fig 2H), supporting the polysome profile data. Taken together, these data are consistent with the notion that p53 mediates mTORC1 inhibition in response to doxorubicin.

mTOR inhibition enhances eIF2α phosphorylation

Communication between mTOR and eIF2 signalling pathways has recently been described (*12–15*), which enables the co-ordination of TC with eIF4F formation in response to cellular stress or growth stimulation. Importantly, our data show that mTORC1 inhibition preceded the phosphorylation of eIF2α after treatment with doxorubicin, suggesting that mTORC1 could regulate eIF2α phosphorylation in response to DNA damage. To investigate this further, both $p53^{+/+}$ and $p53^{-/-}$ MCF10A cells were treated with either doxorubicin or the catalytic mTORC1/2

inhibitor AZD8055. The data show that $p53^{-/-}$ cells lost the capacity to enhance eIF2α phosphorylation in response to doxorubicin (Figs. 3A and 3B), suggesting that mTOR inhibition was required for doxorubicin-induced eIF2α phosphorylation. The phosphorylation of eIF2α was still enhanced in $p53^{-/-}$ cells in response to catalytic mTOR inhibition (Figs. 3A and 3B), indicative of functional signalling downstream of mTOR. These data strongly suggest that p53-dependent mTOR inhibition was critical for the subsequent phosphorylation of eIF2α.

To further explore the correlation between mTOR signalling and eIF2α phosphorylation, MCF10A $p53^{+/+}$ cells were treated with the mTORC1/2 inhibitors Torin 1 and AZD8055, or the allosteric mTORC1 inhibitor Rapamycin. The phosphorylation of eIF2α is enhanced after treatment with all three mTOR inhibitors between 3-6 hours (Fig 3C), which corresponds to the delay observed between mTORC1 inhibition and eIF2α phosphorylation in response to doxorubicin (Fig 1D). To confirm that doxorubicin inhibited mTORC1 and not mTORC2, MCF10A $p53^{+/+}$ cells were treated with either doxorubicin or the catalytic mTORC1/mTORC2 inhibitor AZD8055, and mTORC2-dependent phosphorylation of Akt (at residue S-473) was monitored by immunoblot analysis. As expected, treatment with AZD8055 reduced phosphorylation of Akt at S-473, however, Akt phosphorylation was unaffected following treatment with doxorubicin (Fig S3A), strongly suggesting that doxorubicin inhibited mTORC1.

To determine if mTOR-eIF2 crosstalk signalling was also functional in tumour cells, the mechanism was investigated in a range of cancer cell lines. Using the lung cancer cell line, A549, the data show that doxorubicin inhibited mTORC1 signalling and that both doxorubicin and AZD8055 significantly enhanced eIF2α phosphorylation (Figs 3Di and 3Dii). Moreover, mTOR-eIF2 crosstalk signalling mechanism was also present in HeLa cells (Fig S3B). Furthermore, in support of data obtained in MCF10A cells, siRNA knockdown of p53 in A549 cells abolished both doxorubicin-induced mTORC1 inhibition and eIF2α phosphorylation, whereas AZD8055-induced eIF2α phosphorylation was maintained (Figs 3Ei and 3Eii).

The breast cancer cell line BT474 contains a temperature sensitive p53 mutation within the DNA binding domain that results in impaired p53 function (*36*). Therefore, to further validate the functional role of p53 and mTOR-eIF2 crosstalk signalling in tumour cells, we incubated cells at 37^{o}c to maintain the inactivating p53 mutation or at 32^{o}c to restore p53 function. As expected, doxorubicin treatment did not inhibit mTORC1 signalling or enhance the phosphorylation of eIF2α at 37^{o}c when mutant p53 was present (Figs 3Fi and 3Fii). However, when p53 function was restored at 32^{o}c, treatment with doxorubicin inhibited mTORC1 signalling and subsequently enhanced the phosphorylation of eIF2α (Figs 3Fi and 2Fii). Taken together, these data strongly suggest that mTORC1-eIF2 crosstalk signalling is a general mechanism found in many different tissue or cell types and importantly is functional in tumour cells.

In MEFs, it has been reported previously that inhibition of mTORC1 leads to the activation of GCN2, via the removal of an inhibitory phosphorylation site by protein phosphatase 6 (PP6) (*13*). To address the role of PP6 in human p53$^{+/+}$ MCF10A cells, the catalytic component of PP6, PP6c, was depleted using a specific siRNA. The data show that inactivation of PP6 abolished both doxorubicin- and AZD8055-dependent phosphorylation of eIF2α without reversing mTOR inhibition (Fig S4A), and suggest that PP6 may mediate the signalling response downstream of mTOR in response to DNA damage, consistently with other studies (*13*). However, it is challenging to assign a precise role to PP6 in this pathway given its wide range of functions (*37*) and the fact that PP6c knock-down also has an inhibitory effect on global protein synthesis rates under control conditions (Fig S4B).

mTOR-induced eIF2α phosphorylation is mediated by GCN2 and PERK

Having established that DNA damage-dependent eIF2α phosphorylation requires mTORC1 inhibition, it was important to determine the identity of the relevant eIF2 kinase. To answer this question, we used specific siRNAs to deplete the predominant eIF2Ks in MCF10A cells: PERK, GCN2 and PKR (Fig 4A). AZD8055-induced eIF2α phosphorylation was diminished

after depletion of either GCN2 or PERK, whereas depletion of PKR had a minimal effect (Fig 4B). Moreover, combined reduction of GCN2 and PERK unsurprisingly resulted in the greatest reduction of eIF2α phosphorylation after treatment with AZD8055, but the simultaneous depletion of GCN2, PERK and PKR did not impair the phosphorylation of eIF2α further (Fig 4C). These data are consistent with previous studies (*13*), in that GCN2 enhances the phosphorylation of eIF2α after prolonged mTOR inhibition; however, in human MCF10A cells, PERK was also capable of enhancing eIF2α phosphorylation. Surprisingly, individual depletion of eIF2Ks did not diminish doxorubicin-induced eIF2α phosphorylation (Figs 4Di and 4Dii), although this was achieved with combined depletion of PERK and GCN2 (Fig 4E). In this case, the reduction of AZD8055- and doxorubicin-induced eIF2α phosphorylation was comparable, suggesting that both AZD8055 and doxorubicin promote crosstalk signalling via a common mechanism.

Crosstalk between mTOR and eIF2 is required for cell migration

A range of inhibitors targeting the eIF2 axis in cancers, either as a single agent or as combination therapies, are currently under development. However, the function of eIF2α phosphorylation in protein synthesis regulation is complex and very dependent on cell context. Thus in advanced prostate cancer, eIF2α phosphorylation with loss of PTEN was shown to be associated with poor patient survival (*23*), whereas in malignant melanoma it is associated with resistance to anti-PD-1 immunotherapy and increased cell migration (*22*). We therefore addressed how the crosstalk between eIF2 and mTOR pathways following treatment with the cytotoxic chemotherapeutic doxorubicin could impact upon cell migration.

Trazodone is an anti-depressant which has been recently repurposed to treat neurodegeneration in mice (*38*). Like ISRIB, trazodone relieves eIF2α phosphorylation-mediated translational repression. However, whereas ISRIB functions by enhancing eIF2B activity, it has been suggested that trazodone acts more directly to minimise the reduction of TC in response to eIF2α phosphorylation (Fig 5A) (*38*). Therefore, we used both chemical

compounds to determine the role of eIF2α phosphorylation in the regulation of cell migration in a wound healing assay. Importantly, treatment of MCF10A $p53^{+/+}$ cells with doxorubicin causes cell cycle arrest at both G1/S and G2/M checkpoints (Figs 5B and S5B) and eIF2α phosphorylation was maintained after treatment with doxorubicin for up to 72 hours (Fig S5A). Therefore, MCF10A $p53^{+/+}$ cells were treated for 24 hours with doxorubicin in combination with ISRIB or trazodone, prior to inflicting the wound. Untreated cells start to migrate back into the wound within 48 hours (Fig 5C), and as expected, the migration of doxorubicin-treated cells is slower compared to untreated cells (reduced by ~70%) (Figs 5C and Fig 5D). However, consistent with a role for eIF2 signalling in migration following DNA damage, cells treated with doxorubicin and ISRIB show an even greater inhibition of migration into the wound (reduced by ~85%) compared to untreated cells (Figs 5C and 5D). Moreover, combining doxorubicin and trazodone almost completely abolishes cell migration and significantly reduces migration compared to treatment with doxorubicin alone (Figs 5C and Fig 5D). Doxorubicin induced a small but significant amount of cell death after 72 hours (Fig 5E), however, this small amount of death was unlikely to be sufficient to induce the observed changes in migration. Moreover, doxorubicin-induced cell cycle arrest was maintained after 72 hours in the presence of both ISRIB and trazodone (Fig 5F), strongly suggesting that observed changes in migration were not dependent on cell cycle regulation.

As the inhibition of wound healing was greater using a combination of doxorubicin with trazodone, and that trazodone is already FDA approved with more clinical potential than ISRIB, the migration of cells treated with doxorubicin and trazodone was quantified using the xCELLigence RTCA DP instrument. This technique enables the real-time label free quantification of cell movement from an upper chamber (containing low serum media) to a lower chamber (containing high serum media). As cells migrate through a microporous membrane they pass over microelectrodes which measures impedance and enables the quantification of cell movement. MCF10A $p53^{+/+}$ cells were treated with doxorubicin in combination with trazodone for 24 hours prior to seeding onto the xCELLigence RTCA DP

instrument and migration was quantified for 48 hours. Consistent with the data obtained from the wound healing assay, doxorubicin significantly reduced cell migration compared to untreated cells (Figs. 5G and 5H), and importantly, co-treatment of doxorubicin with trazodone again significantly reduces cell migration compared to cells treated with only doxorubicin (Fig 5H).

As doxorubicin-induced mTOR-eIF2 crosstalk signalling was shown to be functional in A549 cells (Fig 3D and Fig 3E), and that eIF2α phosphorylation was maintained up to 72 hours after treatment (Fig S5C), the rate of A549 cell migration was analysed using the xCELLigence RTCA DP instrument. Interestingly, A549 cells treated with doxorubicin showed a greater capacity to migrate than MCF10A cells, albeit to a lesser extent than untreated cells (Figs 5I and Fig 5J). Importantly, in support of data obtained from MCF10A cells, co-treating A549 cells with doxorubicin and trazodone significantly inhibited cell migration (Figs 5I and Fig 5J). A549 cells were more sensitive to doxorubicin-induced cell death at 72 hours (Fig S5D), however, the non-significant difference in cell death between cells treated with doxorubicin and co-treatment with trazodone were also unlikely to induce the significant inhibition of cell migration. Moreover, cell cycle arrest was maintained in A549 cells treated with doxorubicin and co-treatment with trazodone for up to 72 hours (Figs S5E and S5F), strongly suggesting that changes in migration were not dependent on differential cell cycle regulation.

Taken together these findings indicate that eIF2α phosphorylation promotes the migration of cells in response to doxorubicin, perhaps via translational reprogramming that may enable tumour cell adaptation, and thus have implications for survival rate of patients with certain types of cancers and could provide new therapeutic avenues to limit cancer migration and metastasis.

Discussion

As part of the response to cell stress, eIF4F complex and TC formation are co-ordinated to permit reprogramming of the translatome (*12*), a process which is frequently utilised by tumour cells to promote survival programmes following exposure to cytotoxic chemotherapeutics. mTOR inhibitors including rapamycin, temsirolimus and everolimus, have been used clinically to block translation reprogramming mediated through eIF4F, however in comparison, little work has been carried out to assess the modulation TC formation. Herein, we describe a new regulatory pathway downstream of p53, whereby crosstalk via mTOR to eIF2α phosphorylation, following DNA damage, is required for cell migration (Fig 6). Moreover, blocking this pathway by chemical intervention limits cell migration, supporting the notion that therapeutic targeting of eIF2α signalling to minimise tumour cell metastasis and invasion, could be of therapeutic benefit to specific groups of cancer patients (Fig 6).

In comparison to other studies, e.g. UVB-induced DNA damage (*9*, *10*), we show that there is an extensive delay in the reduction of protein synthesis rates following doxorubicin treatment and an increase in eIF2α phosphorylation. Additionally, our data show that the shutdown of mRNA translation occurs through inhibition of mTORC1, and that this is, in part, dependent on transcriptional pathways induced by p53. It has been shown previously in MEFs that p53-dependent Sestrin2 expression regulates the inhibition of mTORC1 signalling, and de-phosphorylation of 4E-BPs, in response to DNA damage induced by etoposide and cisplatin (*39*). Moreover, depletion of Sestrin1 and Sestrin2 in MCF10A cells abolished IR-mediated protein synthesis inhibition (*40*). Here, Sestrin2 expression was enhanced after treatment with doxorubicin, but abolished after knockout or depletion of p53 and correlating with the relief of mTOR inhibition (Fig 2B and 2D). Moreover, doxorubicin-induced mTORC1 inhibition was independent of TSC, which inhibits mTORC1 by regulating levels of RHEB-GTP. These data are consistent with the notion that doxorubicin could inhibit mTOR signalling via the expression of Sestrin proteins, which can regulate the translocation of mTOR to the lysosome for activation (*41*), however this requires further investigation.

Our results demonstrate that doxorubicin-dependent crosstalk signalling from mTOR to eIF2 requires GCN2 and PERK, and suggest a role for PP6 in this process (Fig 6). These data are broadly consistent with previous studies, albeit using different inducers of cell stress. For example, catalytic inhibition of mTORC1 was shown to increase the activity of PP6, which through the removal of an inhibitory phosphorylation site on GCN2, enhanced eIF2α phosphorylation (*13*). In this case, the co-ordination of mTOR inhibition and eIF2α phosphorylation induced autophagy. Interestingly, mutations of PP6c which promote stabilisation of this protein, and are linked to therapeutic resistance in melanoma, also induce autophagy (*37*). Moreover, a previous study has suggested that in melanoma, cell stress caused by the tumour microenvironment promotes an evolutionarily conserved starvation response requiring eIF2α phosphorylation, which results in cell migration and invasion (*22*). Our data show that crosstalk signalling following doxorubicin-induced DNA damage results in cell migration. Importantly, inhibition of this pathway with either ISRIB or Trazadone, blocks cell migration, suggesting that these compounds would be of therapeutic benefit to block metastasis.

When treating patients with chemotherapeutics that inhibit protein synthesis it is essential to understand the degree of crosstalk between mTOR and eIF2K signalling. Moreover, it is also important to examine how combination therapies, which include the inhibition of the distinct arms of pathways that signal to protein synthesis, impact on cell fate. The data obtained thus far suggests that the degree of crosstalk from mTOR to eIF2K signalling is dependent on a range of factors including the DNA damaging agent used and acquired mutation status of the tumour. Our data strongly suggest that combination therapy, including an agent that blocks crosstalk signalling from mTOR to eIF2α phosphorylation, holds great potential to reduce migration and metastasis. However, there needs to be careful patient stratification, in terms of the DNA-damaging agent used and an understanding of the how these signalling pathways are activated in the tumour samples to ensure effectiveness of such treatments.

Materials and Methods

Cell culture

MCF10A cells are a non-transformed human breast epithelial cell line. MCF10A cells were cultured in Dulbecco's modified Eagle's medium (DMEM)/F12 (1:1) supplemented with horse serum (5%), recombinant human EGF (20 ng/ml), human insulin (10 μg/ml), hydrocortisone (500 ng/ml) and cholera toxin (10 ng/ml). p53 wild-type MCF10A ($p53^{+/+}$) cells were obtained from ATCC and p53 knockout MCF10A ($p53^{-/-}$) cells were obtained from Sigma. A549, HeLa and BT474 cell lines were obtained from ATCC and cultured in Dulbecco's modified Eagle's medium (DMEM) supplemented with 10% FBS.

Treatment of cells

DNA damage was induced by treating cells with doxorubicin (500 nM or 1 μM) (Sigma) for 0-48 hours. mTOR was catalytically inhibited by treating cells with AZD8055 (100 nM) (Selleckchem), Torin 1 (100 nM) (Cell Signalling Technologies) or Rapamycin (100 nM) (Cell Signalling Technologies) for 0-24 hours. Cells were treated with Thapsigargin (250 nM) (Sigma) for 1 hour to induce ER stress, and treated with ISRIB (200 nM) (Sigma) or Trazodone (50 μM) (Sigma) to reverse the effects eIF2α phosphorylation.

Cell transfections

Cells were transfected with siRNAs using lipofectamine RNAiMAX reagent (Invitrogen) in 6-well plates as per manufacturer guidelines for 24-72 hours. ON-TARGETplus siRNAs purchased from Dharmacon: GCN2 (LQ-005314-00-0002), PERK (LQ-004883-00-0002), PKR (LQ-003527-00-0002), PP6c (LQ-009935-00-0002), TSC2 (LQ-003029-00-0002), and non-targeting siRNA (D-001810-01-05). siRNA specific for p53 was purchased from ThermoFisher scientific (Silencer select siRNA, catalogue number: 4390825).

Western blot analysis

Whole cell extracts were prepared in lysis buffer (50 mM Tris pH 7.5, 150 mM sodium chloride, 1% Triton X-100, 0.1% SDS, 0.5% sodium deoxycholate, 1X Roche protease inhibitor cocktail and 1X Roche PhosStop phosphatase inhibitor cocktail) and protein concentration of each sample was quantified using Pierce BCA protein assay kit (ThermoFisher scientific). Extracts were diluted in SDS loading buffer (50 mM Tris pH 6.8, 2% SDS, 10% glycerol, 0.1% bromophenol blue, 50 mM DTT) and total protein (20-30 μg) was separated according to mass using sodium dodecyl sulphate polyacrylamide gel electrophoresis (SDS-PAGE). Proteins were transferred to PVDF membrane and incubated with the appropriate antibody at the manufacturers recommended dilution. Primary antibodies used: eIF2α (CST, #9772), phospho-eIF2α (S-51) (Abcam, #32157), phospho-4E-BP1 (S-65) (CST, #9456), 4E-BP1 (CST, #9644), phospho-p70 S6K (T-389) (CST, #9205), p70 S6K (CST, #2708), p-Akt (S-473) (CST, #4058), Akt (CST, #9272), p53 (Dako, #M7001), Sestrin 2 (Abcam, ab178518), phospho-ATM (S-1981) (Abcam, #81292), ATM (Abcam, #32420), phospho-Chk 2 (T-68) (CST, #2661), Chk 2 (#2662), GCN2 (CST, #3302), PKR (CST, #12297), PERK (CST, #3192), ATF-4 (CST, #11815), PP6c (Abcam, #131335), TSC2 (CST, #4308S), BIP (Proteintech, #11587-1-AP), CHOP (Proteintech, #15204-1-AP) and β-tubulin (CST, #2146).

For ECL detection, membranes were incubated with HRP-conjugated α-mouse (Dako, #P0447) or α-rabbit (GE healthcare, #NA934V) secondary antibodies. Signal was developed by incubating membranes in ECL-prime solution for 5 minutes, and X-ray film was exposed to the membrane to visualize luminescence. For LI-COR detection, membranes were incubated with IR-dye labelled α-mouse (CST, #5257S) or α-rabbit (CST, #5366S) secondary antibodies. Fluorescent signal was detected using LI-COR Odyssey imaging system (LI-COR biosciences) and images analysed with LI-COR image studio software (package version 5.2.5). Quantification of signal from both ECL and LI-COR detected blots was carried out using LI-COR image studio.

Sucrose density centrifugation

Sucrose gradients were used to separate subpolysomal and polysomal ribosomes. 10%-50% (w/v) sucrose gradients were prepared in gradient buffer (300 mM NaCl2, 15 mM MgCl2, 15 mM tris-HCL pH 7.5, 1 mM DTT, 0.1 mg/ml cycloheximide). Cells were seeded on a 15 cm dish, washed in PBS-cyclohexamide (100 μg/ml), and scraped into lysis buffer (300 mM NaCl2, 15 mM MgCl2, 15 mM tris-HCL pH 7.5, 1 mM DTT, 0.2 M sucrose, 0.1 mg/ml cycloheximide, 0.5% IGEPAL, 5 μl RNasin per 1 ml). Lysates were incubated on ice for three minutes prior to pelleting cells at 1300 x g for 5 minutes. The supernatant was layered onto the gradient and centrifuged at 38,000 rpm (acceleration 9, deceleration 6) for 2 hours at 4^{o}C using a Beckman Coulter ultracentrifuge. Gradients were fractioned using a gradient fractionation system (Presearch Ltd) and fractions were collected at 1 minute intervals using FOXY Jr collection system (Presearch Ltd), at a flow rate of 1 ml/minute. Absorbance was measured constantly at 254 nm using a UA-6 UV-VIS detector (Presearch Ltd). The relative rate of translation was estimated by calculating a ratio of polysomes/subpolysomes, by measuring the area under the curve within the subpolysomes (fractions 1-5) and the polysomes (fractions 6-10).

Radioisotope incorporation

For $^{[35]}$S-methionine incorporation, cells were incubated with radiolabelled $^{[35]}$S-methionine for 30 minutes at normal cell culture conditions. Cells were washed with PBS and lysed with passive lysis buffer (Promega). For $^{[3]}$H-uridine incorporation, cells were incubated with radiolabelled $^{[3]}$H-uridine for 30 minutes at normal growth conditions. Cells were washed with PBS and lysed with whole cell lysis buffer. Protein was precipitated using trichloroacetic acid (TCA) at a final concentration of 25% and protein was captured on glass fibre filter paper (GE Healthcare). Captured protein was washed with 70% IMS and acetone prior to the addition of 2 ml ecoscint scintillation cocktail (National Diagnostics) and radioisotope incorporation was quantified using a Wallac winspectral 1414 liquid scintillation counter. Each sample was carried out in triplicate and spectral counts per minute were normalised to the total amount of protein for each sample.

Flow cytometry

All treatments were carried out using a 6-well plate and all flow cytometry data was acquired using BD FACS Aria II, BD FACS Canto II and BD LSRFortessa (BD bioscience). 10,000 counts were acquired for each experimental condition and all flow cytometry data was analysed with FlowJo data analysis software (version 10.1) (FlowJo LLC, Ashland, USA).

Cell death was quantified by measuring Annexin-V-FITC binding to externalized phosphatidylserine (with a 488 nM laser), and Draq7 uptake in the cell (with a 561 nM laser). Cells were collected and washed in PBS prior to resuspension in annexin buffer (BD bioscience) and incubation with Annexin-V and Draq7 for 20 minutes prior to analysis.

For cell cycle analysis, cells were incubated with the thymidine analogue 5-ethynyl-2'-deoxyuridine (EdU) (20 μM) for 90 minutes to quantify cells within S-phase; and FxCycle violet stain (4', 6-diamidino-2-phenylindole, dihydrochloride), which binds to double-stranded DNA, to determine populations of cells within G1 and G2 phases of the cell cycle. Cells were collected and fixed in ice cold 70% ethanol. EdU incorporation within fixed cells was quantified using Click-iT EdU Flow Cytometry Assay Alexa Fluor 647 azide (Life technologies), following manufacturers protocol, and detected with a 640 nM laser. To additionally quantify the population of cells within G1 and G2 stages of the cell cycle, FxCycle violet stain (Invitrogen) was incubated with EdU incorporated cells for 16 hours at 4^{o}C and detected with a 405 nM laser.

Cell migration and scratch assay

Cell migration assays were performed in a standard CO_2 incubator using the xCELLigence RTCA DP instrument (ACEA Biosciences) according to manufacturer's instructions. Briefly, $3x10^4$ MCF10A cells and $2.5x10^4$ A549 cells were seeded in the upper chamber of a 16 well migration plate (CIM-16 plate) in 100 μl of media containing only 0.1% serum. Cells migrate to a lower chamber containing 160 μl of supplemented media via a microporous membrane.

Microelectrode sensors are embedded on the underside of the microporous membrane. As cells move across the microelectrodes into the lower chamber, they generate impedance measurements which enables label free quantification of cell migration. Cells were treated with the indicated compounds for 24 hours prior to seeding, and migration was continuously monitored in real time for 48 hours.

For wound healing assays, cells were grown to confluence and treated with the indicated compounds for 24 hours prior to a scratch being made with a p200 pipette tip. The migration of cells back into the wounded area was monitored using phase contrast optics and a Zeiss Axiovert 200M microscope after 48 hours. A percentage of wound closure (*42*) was calculated by quantifying the area of the wounds at 0 hours and 48 hours using Image J.

Statistical analysis

All statistical analysis testing for significance used an unpaired student's *t*-test. A *P*-value <0.05 (*), <0.01 (**) and <0.001 (***) were considered to be statistically significant from three independent experiments.

Supplementary Materials

Figure S1. Doxorubicin inhibited protein synthesis and induced cell death In MCF10A cells.

Figure S2. Doxorubicin-induced mTOR inhibition was not dependent on TSC activity.

Figure S3. Doxorubicin inhibits mTORC1 signalling

Figure S4. Knockdown of PP6 activity reduced protein synthesis rates

Figure S5. eIF2α-mediated cell migration was not caused by changes in cell death or cell cycle regulation

References

1. F. Buttgereit, M. D. Brand, A hierarchy of ATP-consuming processes in mammalian cells. *Biochemical Journal*. **312**, 163–167 (1995).

2. K. A. Spriggs, M. Bushell, A. E. Willis, Translational Regulation of Gene Expression during Conditions of Cell Stress. *Molecular Cell*. **40**, 228–237 (2010).

3. A. G. Hinnebusch, The scanning mechanism of eukaryotic translation initiation. *Annual Review of Biochemistry*. **83**, 779–812 (2014).

4. S. Mader, H. Lee, A. Pause, N. Sonenberg, The translation initiation factor eIF-4E binds to a common motif shared by the translation factor eIF-4 gamma and the translational repressors 4E-binding proteins. *Molecular and Cellular Biology*. **15**, 4990–7 (1995).

5. R. A. Saxton, D. M. Sabatini, mTOR Signaling in Growth Control and Disease. *Cell*. **168**, 960–976 (2017).

6. A. Gingras, B. Raught, N. Sonenberg, Regulation of translation initiation by FRAP / mTOR. *Genes & Development*. **15**, 807–826 (2001).

7. J. Somers, T. Pöyry, A. E. Willis, A perspective on mammalian upstream open reading frame function. *International Journal of Biochemistry and Cell Biology*. **45**, 1690–1700 (2013).

8. N. Donnelly, A. M. Gorman, S. Gupta, A. Samali, The eIF2α kinases: Their structures and functions. *Cellular and Molecular Life Sciences*. **70**, 3493–3511 (2013).

9. J. Deng, H. P. Harding, B. Raught, A. C. Gingras, J. J. Berlanga, D. Scheuner, R. J. Kaufman, D. Ron, N. Sonenberg, Activation of gcn2 in uv-irradiated cells inhibits translation. *Current Biology*. **12**, 1279–1286 (2002).

10. I. R. Powley, A. Kondrashov, L. A. Young, H. C. Dobbyn, K. Hill, I. G. Cannell, M.

Stoneley, Y. W. Kong, J. A. Cotes, G. C. M. Smith, R. Wek, C. Hayes, T. W. Gant, K. A. Spriggs, M. Bushell, A. E. Willis, Translational reprogramming following UVB irradiation is mediated by DNA-PKcs and allows selective recruitment to the polysomes of mRNAs encoding DNA repair enzymes. *Genes and Development*. **23**, 1207–1220 (2009).

11. J. Somers, L. A. Wilson, J. P. Kilday, E. Horvilleur, I. G. Cannell, T. A. A. Pöyry, L. C. Cobbold, A. Kondrashov, J. R. P. Knight, S. Puget, J. Grill, R. G. Grundy, M. Bushell, A. E. Willis, A common polymorphism in the 5' UTR of ERCC5 creates an upstream ORF that confers resistance to platinum-based chemotherapy. *Genes and Development*. **29**, 1891–1896 (2015).

12. V. Gandin, L. Masvidal, M. Cargnello, L. Gyenis, S. McLaughlan, Y. Cai, C. Tenkerian, M. Morita, P. Balanathan, O. Jean-Jean, V. Stambolic, M. Trost, L. Furic, L. Larose, A. E. Koromilas, K. Asano, D. Litchfield, O. Larsson, I. Topisirovic, mTORC1 and CK2 coordinate ternary and eIF4F complex assembly. *Nature Communications*. **7**, 11127 (2016).

13. J. Wengrod, D. Wang, S. Weiss, H. Zhong, I. Osman, L. B. Gardner, Phosphorylation of eIF2α triggered by mTORC1 inhibition and PP6C activation is required for autophagy and is aberrant in PP6C-mutated melanoma. *Science Signaling*. **8**, 27 (2015).

14. K. Rajesh, J. Krishnamoorthy, U. Kazimierczak, C. Tenkerian, A. I. Papadakis, S. Wang, S. Huang, A. E. Koromilas, Phosphorylation of the translation initiation factor eIF2α at serine 51 determines the cell fate decisions of Akt in response to oxidative stress. *Cell Death & Disease*. **6**, e1591 (2015).

15. J. Krishnamoorthy, C. Tenkerian, J. Gupta, N. Ghaddar, S. Wang, C. Darini, K. A. Staschke, A. Ghosh, V. Gandin, I. Topisirovic, A. S. Kristof, M. Hatzoglou, G. Simos, A. E. Koromilas, Downregulation of PERK activity and eIF2α serine 51

phosphorylation by mTOR complex 1 elicits pro-oxidant and pro-death effects in tuberous sclerosis-deficient cells article. *Cell Death and Disease*. **9**, 1–12 (2018).

16. C. Tenkerian, J. Krishnamoorthy, Z. Mounir, U. Kazimierczak, A. Khoutorsky, K. A. Staschke, A. S. Kristof, S. Wang, M. Hatzoglou, A. E. Koromilas, mTORC2 balances Akt activation and eIF2alpha serine 51 phosphorylation to promote survival under stress. *Molecular Cancer Research*. **1**, 1377–1388 (2015).

17. Y. Martineau, R. Azar, C. Bousquet, S. Pyronnet, Anti-oncogenic potential of the eIF4E-binding proteins. *Oncogene*. **32**, 671–677 (2012).

18. C. de la Parra, B. A. Walters, P. Geter, R. J. Schneider, Translation initiation factors and their relevance in cancer. *Current Opinion in Genetics & Development*. **48**, 82–88 (2018).

19. L. M. Lindqvist, K. Tandoc, I. Topisirovic, L. Furic, Cross-talk between protein synthesis , energy metabolism and autophagy in cancer. *Current Opinion in Genetics & Development*. **48**, 104–111 (2018).

20. J. W. Moroney, M. P. Schlumbrecht, T. Helgason, R. L. Coleman, S. Moulder, A. Naing, D. C. Bodurka, F. Janku, D. S. Hong, R. Kurzrock, A phase I trial of liposomal doxorubicin, bevacizumab, and temsirolimus in patients with advanced gynecologic and breast malignancies. *Clinical Cancer Research*. **17**, 6840–6846 (2011).

21. R. K. Basho, M. Gilcrease, R. K. Murthy, T. Helgason, D. D. Karp, F. Meric-Bernstam, K. R. Hess, S. M. Herbrich, V. Valero, C. Albarracin, J. K. Litton, M. Chavez-MacGregor, N. K. Ibrahim, J. L. Murray, K. B. Koenig, D. Hong, V. Subbiah, R. Kurzrock, F. Janku, S. L. Moulder, Targeting the PI3K/AKT/mTOR pathway for the treatment of mesenchymal triple-negative breast cancer: Evidence from a phase 1 trial of mTOR inhibition in combination with liposomal doxorubicin and bevacizumab. *JAMA Oncology*. **3**, 509–515 (2017).

22. P. Falletta, L. Sanchez-del-Campo, J. Chauhan, M. Effern, A. Kenyon, C. J. Kershaw, R. Siddaway, R. Lisle, R. Freter, M. J. Daniels, X. Lu, T. Tüting, M. Middleton, F. M. Buffa, A. E. Willis, G. Pavitt, Z. A. Ronai, T. Sauka-Spengler, M. Hölzel, C. R. Goding, Translation reprogramming is an evolutionarily conserved driver of phenotypic plasticity and therapeutic resistance in melanoma. *Genes and Development*. **31**, 18–33 (2017).

23. H. G. Nguyen, C. S. Conn, Y. Kye, L. Xue, C. M. Forester, J. E. Cowan, A. C. Hsieh, J. T. Cunningham, C. Truillet, F. Tameire, M. J. Evans, C. P. Evans, J. C. Yang, B. Hann, C. Koumenis, P. Walter, P. R. Carroll, D. Ruggero, Development of a stress response therapy targeting aggressive prostate cancer. *Science Translational Medicine*. **10**, 1–12 (2018).

24. D. A. Gewirtz, A critical evaluation of the mechanisms of action proposed for the antitumor effects of the anthracycline antibiotics adriamycin and daunorubicin. *Biochemical Pharmacology*. **57**, 727–741 (1999).

25. F. Yang, S. S. Teves, C. J. Kemp, S. Henikoff, Doxorubicin, DNA torsion, and chromatin dynamics. *Biochimica et Biophysica Acta*. **1845**, 84–89 (2014).

26. J. H. Doroshow, K. J. A. Davies, Redox cycling of anthracyclines by cardiac mitochondria. II. Formation of superoxide anion, hydrogen peroxide, and hydroxyl radical. *Journal of Biological Chemistry*. **261**, 3068–3074 (1986).

27. H. Gaillard, A. Aguilera, A Novel Class of mRNA-containing Cytoplasmic Granules Are Produced in Response to UV-Irradiation. *Molecular Biology of the Cell*. **19**, 4980–4992 (2008).

28. M. T. Moutaoufik, R. El Fatimy, H. Nassour, C. Gareau, J. Lang, R. M. Tanguay, R. Mazroui, E. W. Khandjian, UVC-induced stress granules in mammalian cells. *PLoS ONE*. **9** (2014).

29. C. Sidrauski, D. Acosta-Alvear, A. Khoutorsky, P. Vedantham, B. R. Hearn, H. Li, K. Gamache, C. M. Gallagher, K. K. H. Ang, C. Wilson, V. Okreglak, A. Ashkenazi, B. Hann, K. Nader, M. R. Arkin, A. R. Renslo, N. Sonenberg, P. Walter, Pharmacological brake-release of mRNA translation enhances cognitive memory. *eLife*. **2013**, 1–22 (2013).

30. C. Sidrauski, A. M. McGeachy, N. T. Ingolia, P. Walter, The small molecule ISRIB reverses the effects of eIF2α phosphorylation on translation and stress granule assembly. *eLife*. **4**, 1–16 (2015).

31. S. Dey, T. D. Baird, D. Zhou, L. R. Palam, D. F. Spandau, R. C. Wek, Both transcriptional regulation and translational control of ATF4 are central to the integrated stress response. *The Journal of Biological Chemistry*. **285**, 33165–33174 (2010).

32. L. E. Horton, M. Bushell, D. Barth-Baus, V. J. Tilleray, M. J. Clemens, J. O. Hensold, p53 activation results in rapid dephosphorylation of the eIF4E-binding protein 4E-BP1, inhibition of ribosomal protein S6 kinase and inhibition of translation initiation. *Oncogene*. **21**, 5325–5334 (2002).

33. N. Akeno, A. L. Miller, X. Ma, K. . . Wikenheiser-Brokamp, p53 suppresses carcinoma progression by inhibiting mTOR pathway activation. *Oncogene*. **34**, 1–11 (2015).

34. K. Inoki, Y. Li, T. Xu, K. L. Guan, Rheb GTpase is a direct target of TSC2 GAP activity and regulates mTOR signaling. *Genes and Development*. **17**, 1829–1834 (2003).

35. Z. Feng, H. Zhang, A. J. Levine, S. Jin, The coordinate regulation of the p53 and mTOR pathways in cells. *Proceedings of the National Academy of Sciences of the United States of America*. **102**, 8204–8209 (2005).

36. M. Christgen, M. Noskowicz, C. Heil, E. Schipper, H. Christgen, R. Geffers, H. Kreipe, U. Lehmann, IPH-926 lobular breast cancer cells harbor a p53 mutant with

temperature-sensitive functional activity and allow for profiling of p53-responsive genes. *Laboratory Investigation*. **92**, 1635–1647 (2012).

37. T. Ohama, The multiple functions of protein phosphatase 6. *Biochimica et Biophysica Acta - Molecular Cell Research*. **1866**, 74–82 (2019).

38. M. Halliday, H. Radford, K. A. M. Zents, C. Molloy, J. A. Moreno, N. C. Verity, E. Smith, C. A. Ortori, D. A. Barrett, M. Bushell, G. R. Mallucci, Repurposed drugs targeting eIF2α-P-mediated translational repression prevent neurodegeneration in mice. *Brain*. **140**, 1768–1783 (2017).

39. M. Cam, H. K. Bid, L. Xiao, G. P. Zambetti, P. J. Houghton, H. Cam, P53/TAp63 and AKT regulate mammalian target of rapamycin complex 1 (mTORC1) signaling through two independent parallel pathways in the presence of DNA damage. *Journal of Biological Chemistry*. **289**, 4083–4094 (2014).

40. S. Braunstein, M. L. Badura, Q. Xi, S. C. Formenti, R. J. Schneider, Regulation of protein synthesis by ionizing radiation. *Molecular and Cellular Biology*. **29**, 5645–56 (2009).

41. A. Parmigiani, A. Nourbakhsh, B. Ding, W. Wang, Y. Kim, K. Akopiants, K. L. Guan, M. Karin, A. Budanov, Sestrins Inhibit mTORC1 Kinase Activation through the GATOR Complex. *Cell Reports*. **9**, 1281–1291 (2014).

42. P. Y. K. Yue, E. P. Y. Leung, N. K. Mak, R. N. S. Wong, A Simplified Method for Quantifying Cell Migration/Wound Healing in 96-Well Plates. *Journal of Biomolecular Screening*. **15**, 427–433 (2010).

Acknowledgements

We thank Dr Lucia Pinon and Dr David Read for assistance with flow cytometry and microscopy analysis. We also thank Dr Mariavittoria Pizzinga and Professor Martin Bushell for the critical reading of the manuscript.

Funding

RFH was supported by MRC studentship and Wellcome Trust [grant number: 110071/Z/15/Z]. AEW, TAAP and MS were supported by MRC programme funding [MC_UP_A600_1023].

Author contributions

RFH performed the experiments. RFH, TAAP, MS and AEW designed the experiments and interpreted results. RFH and AEW wrote the manuscript.

Conflict of interest

The authors declare that they have no conflict of interest.

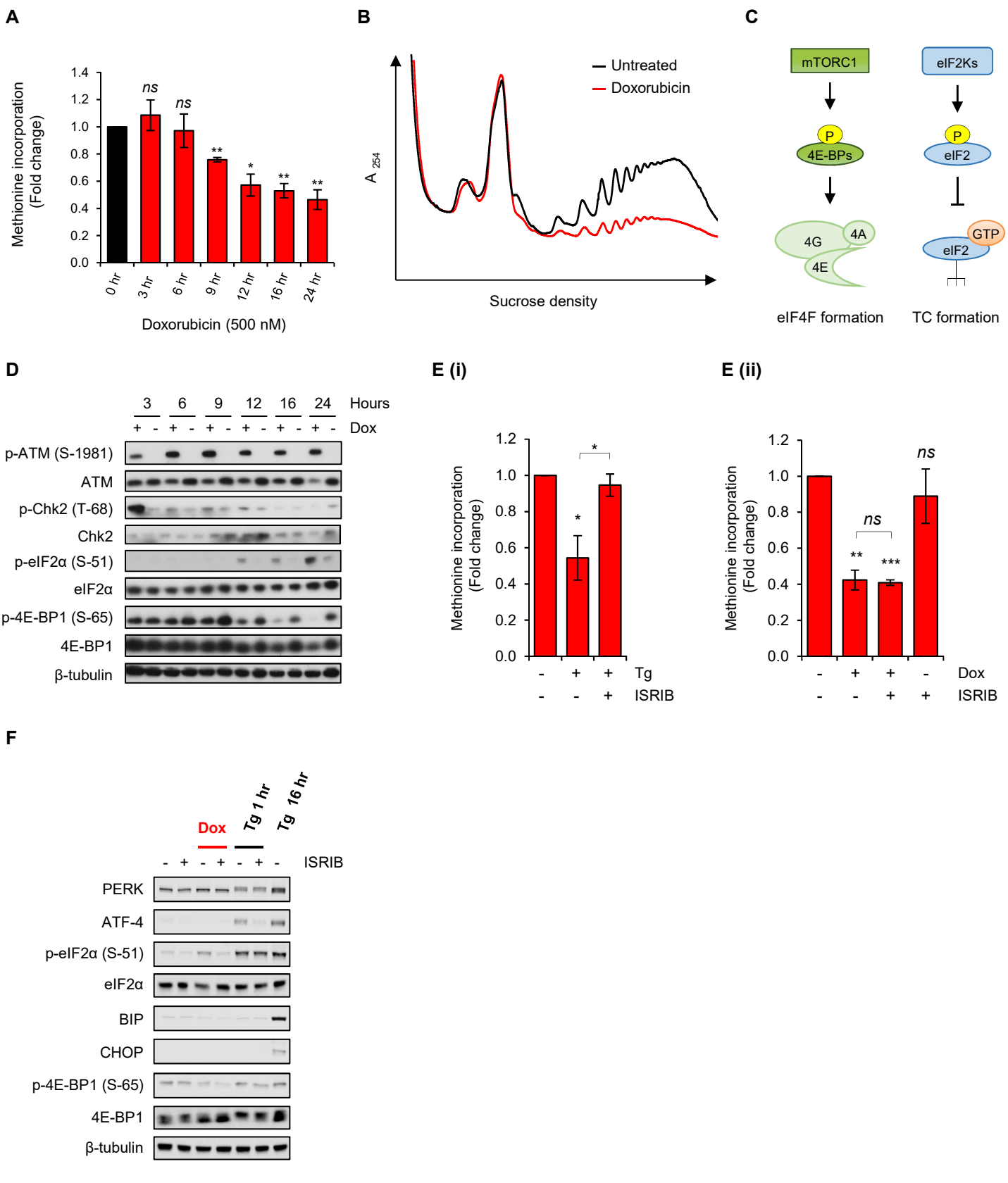
A
Methionine incorporation (Fold change)
1.4
1.2
1.0
0.8
0.6
0.4
0.2
0.0
ns
ns
**
*
**
**
0 hr
3 hr
6 hr
9 hr
12 hr
16 hr
24 hr
Doxorubicin (500 nM)
B
Untreated
Doxorubicin
A 254
Sucrose density
C
mTORC1
eIF2Ks
P
4E-BPs
P
eIF2
4G
4A
4E
GTP
eIF2
eIF4F formation
TC formation
D
3
6
9
12
16
24
Hours
+ - + - + - + - + - + -
Dox
p-ATM (S-1981)
ATM
p-Chk2 (T-68)
Chk2
p-eIF2α (S-51)
eIF2α
p-4E-BP1 (S-65)
4E-BP1
β-tubulin
E (i)
Methionine incorporation (Fold change)
1.2
1.0
0.8
0.6
0.4
0.2
0.0
*
*
- + + Tg
- - + ISRIB
E (ii)
Methionine incorporation (Fold change)
1.2
1.0
0.8
0.6
0.4
0.2
0.0
ns
ns
**
***
- + + - Dox
- - + + ISRIB
F
Dox
Tg 1 hr
Tg 16 hr
- + - + - + - ISRIB
PERK
ATF-4
p-eIF2α (S-51)
eIF2α
BIP
CHOP
p-4E-BP1 (S-65)
4E-BP1
β-tubulin

Figure 1

Figure 1. Doxorubicin-induced DNA damage inhibited global protein synthesis rates.

A. MCF10A cells were treated with doxorubicin (500 nM) for the indicated time and pulse-labelled with $^{[35]}$S-methionine for 30 minutes. Total counts per minute were normalised to total protein and values are shown as a fold change relative to untreated control samples for each time point. Error bars represent mean ± SD (*n* = 3), ***P* = <0.01, **P* = <0.05, by unpaired student's *t*-test (*n.s* = not significant).

B. Comparison of polysome profiles from MCF10A cells untreated or treated continuously with doxorubicin (500 nM) for 24 hours. Cytoplasmic lysates were centrifuged at 38000 rpm through 10%-50% sucrose gradients at 4^{o}C for two hours, and absorbance was measured at 254 nm using a flow rate of 1 ml/min.

C. Schematic representation of the regulation of translation initiation via mTOR-dependent regulation of eIF4F complex formation, and eIF2K-depednent regulation of ternary complex (TC) formation.

D. MCF10A cells were treated with doxorubicin (500 nM) for the indicated time, lysed and analysed by immunoblotting with the indicated antibodies. Blots shown were representative of three independent repeats.

E. (i) MCF10A cells were treated with thapsigargin (250 nM for 1 hour), with or without ISRIB (200 nM), and pulse-labelled with $^{[35]}$S-methionine for 30 minutes. (ii) MCF10A cells were treated with doxorubicin (500 nM for 16 hours), with or without ISRIB (200 nM), and pulse-labelled with $^{[35]}$S-methionine for 30 minutes. Total counts per minute were normalised to total protein and values are shown as a fold change relative to untreated control samples for each time point. Error bars represent mean ± SD (*n* = 3), ****P* = <0.001, ***P* = <0.01, **P* = <0.05, by unpaired student's *t*-test (*ns* = not significant).

F. Samples prepared in parallel to (E) were lysed and analysed by immunoblotting with the indicated antibodies. Blots shown were representative of three independent repeats.

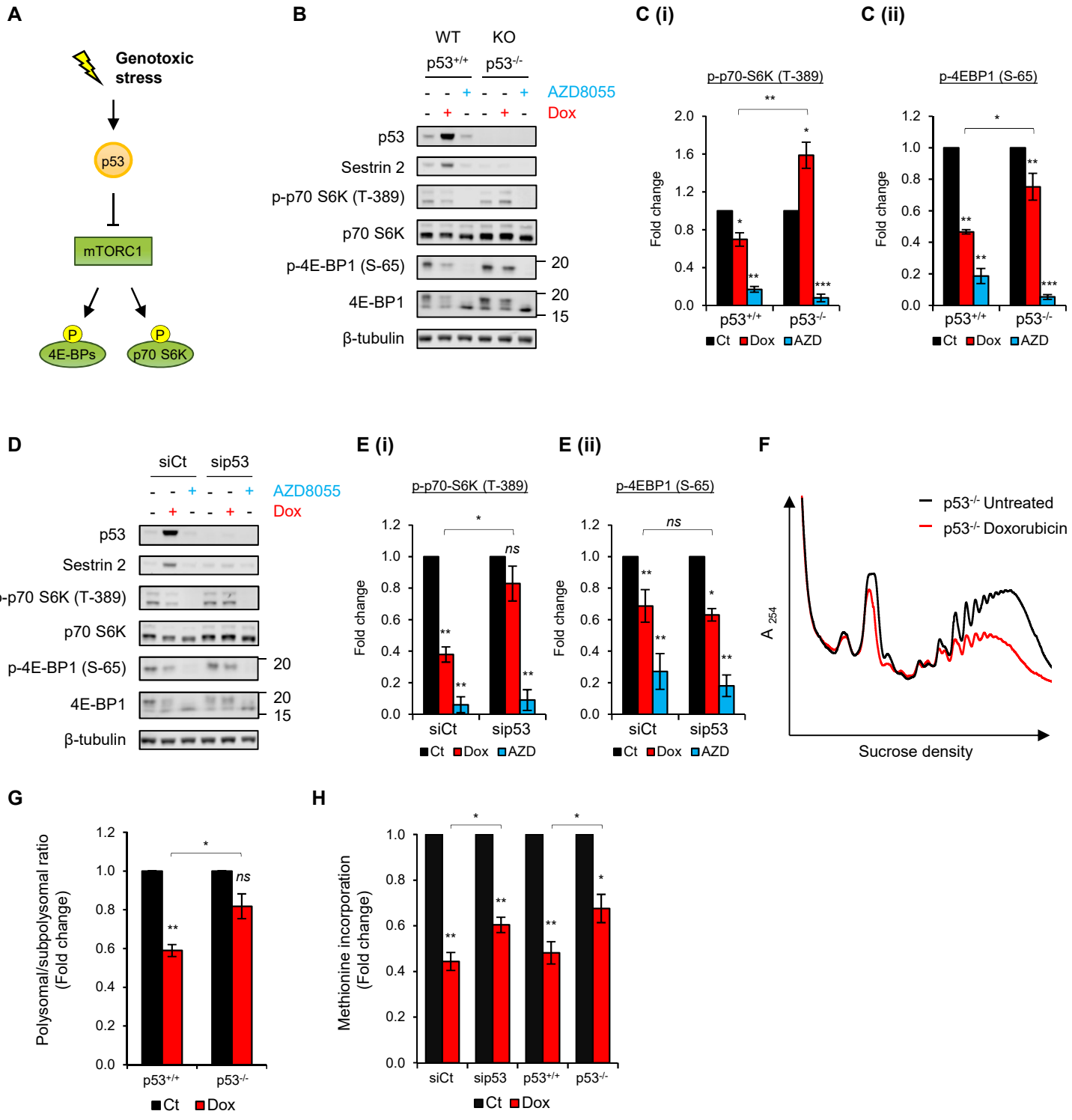
A
Genotoxic stress
p53
mTORC1
P
4E-BPs
P
p70 S6K
B
WT
KO
p53+/+
p53-/-
AZD8055
Dox
p53
Sestrin 2
p-p70 S6K (T-389)
p70 S6K
p-4E-BP1 (S-65)
4E-BP1
β-tubulin
20
20
15
C (i)
p-p70-S6K (T-389)
Fold change
p53+/+
p53-/-
Ct
Dox
AZD
C (ii)
p-4EBP1 (S-65)
Fold change
p53+/+
p53-/-
Ct
Dox
AZD
D
siCt
sip53
AZD8055
Dox
p53
Sestrin 2
p-p70 S6K (T-389)
p70 S6K
p-4E-BP1 (S-65)
4E-BP1
β-tubulin
20
20
15
E (i)
p-p70-S6K (T-389)
Fold change
ns
siCt
sip53
Ct
Dox
AZD
E (ii)
p-4EBP1 (S-65)
Fold change
ns
siCt
sip53
Ct
Dox
AZD
F
p53-/- Untreated
p53-/- Doxorubicin
A254
Sucrose density
G
Polysomal/subpolysomal ratio (Fold change)
ns
p53+/+
p53-/-
Ct
Dox
H
Methionine incorporation (Fold change)
siCt
sip53
p53+/+
p53-/-
Ct
Dox

Figure 2

Figure 2. Doxorubicin-induced mTOR inhibition was dependent on p53 activity

A. Schematic representation depicting the regulation of mTOR signalling. Blocked arrows indicate the inhibition of the following protein, whereas arrows indicate the phosphorylation or activation of the downstream protein.

B. Wild-type p53 MCF10A cells ($p53^{+/+}$) and p53 knockout MCF10A cells ($p53^{-/-}$) were treated with doxorubicin (500 nM) or AZD8055 (100 nM) for 16 hours. Cells were lysed and analysed by immunoblotting with the indicated antibodies. Blots shown were representative of three independent repeats.

C. Quantification of (i) p70 S6K phosphorylation at Thr-389, and (ii) 4E-BP1 phosphorylation at Ser-65 from blots shown in A. Error bars represent mean ± SD (*n* = 3), ****P* = <0.001, ***P* = <0.01, **P* = <0.05, by unpaired student's *t*-test (*ns* = not significant).

D. $p53^{+/+}$ MCF10A cells were transfected with an siRNA specific toward endogenous p53 (sip53) or a non-specific scrambled control siRNA (siCt). Following two consecutive 24-hour transfections, cells were treated with doxorubicin (500 nM) or AZD8055 (100 nM) for 16 hours. Cells were lysed and analysed by immunoblotting with the indicated antibodies. Blots shown were representative of three independent repeats.

E. Quantification of (i) p70 S6K phosphorylation at Thr-389, and (ii) 4E-BP1 phosphorylation at Ser-65 from blots shown in C. Error bars represent mean ± SD (*n* = 3), ***P* = <0.01, **P* = <0.05, by unpaired student's *t*-test (*ns* = not significant).

F. Comparison of polysome profiles from MCF10A $p53^{-/-}$ cells untreated or treated continuously with doxorubicin (500 nM) for 24 hours. Cytoplasmic lysates were centrifuged at 38000 rpm through 10%-50% sucrose gradients at 4°C for two hours, and absorbance was measured at 254 nm using a flow rate of 1 ml/min.

G. Polysome/subpolysomal ratio from $p53^{+/+}$ and $p53^{-/-}$ cells treated with doxorubicin for 24 hours. Ratio was calculated from the area under the curve of polysome profiles

separated into polysomal and subpolysomal regions. Error bars represent mean ± SD (*n* = 3), ***P* = <0.01, **P* = <0.05, by unpaired student's *t*-test (*ns* = not significant).

H. MCF10A $p53^{+/+}$ and $p53^{-/-}$ cells, as well as $p53^{+/+}$ cells transfected with siRNA specific for p53 or a control non-targeting siRNA, were pulse-labelled with $^{[35]}$S-methionine for 30 minutes. Total counts per minute were normalised to total protein and values are shown as a fold change relative to untreated control samples for each time point. Error bars represent mean ± SD (*n* = 3), ***P* = <0.01, **P* = <0.05, by unpaired student's *t*-test.

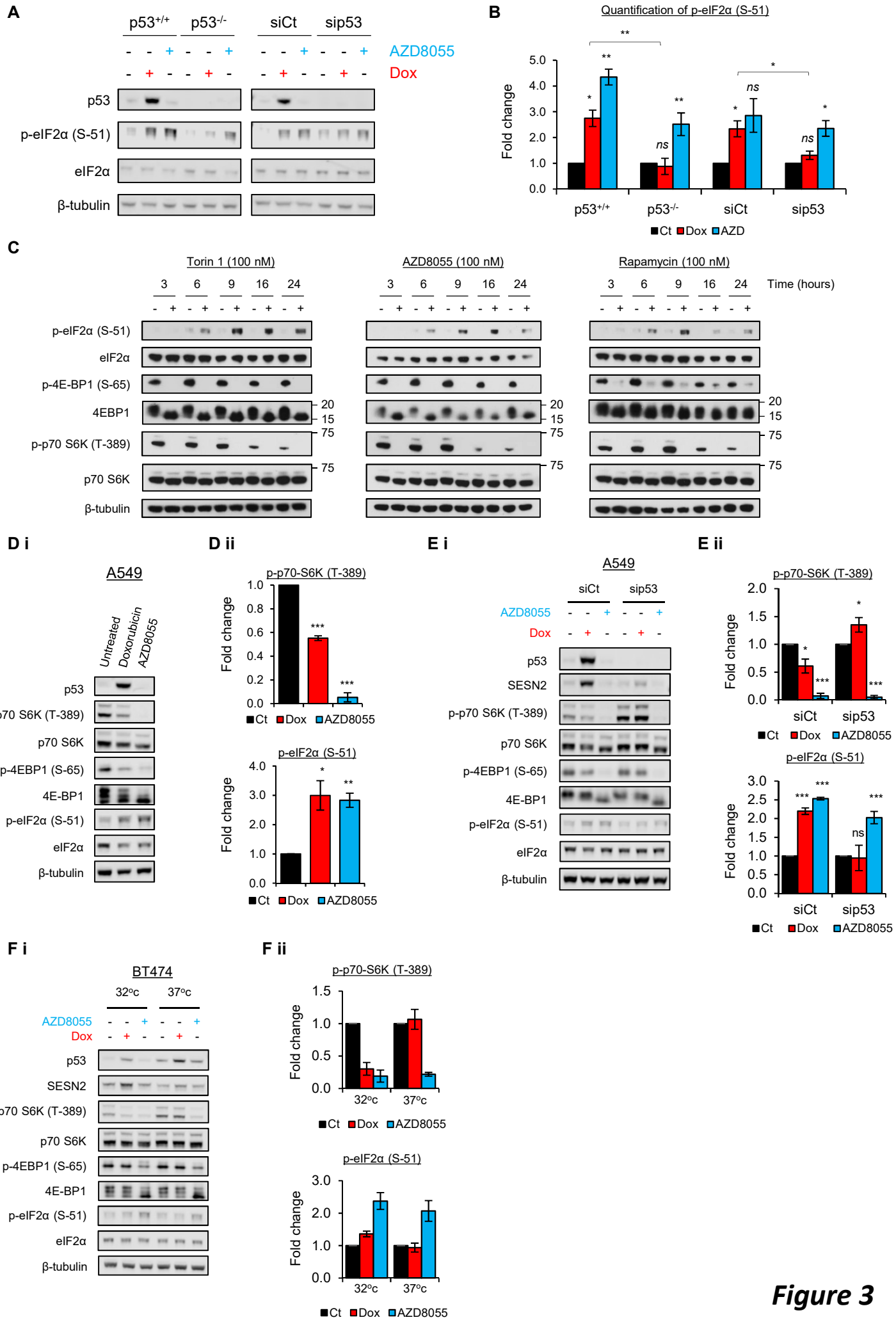
A
p53+/+
p53-/-
siCt
sip53
AZD8055
Dox
p53
p-eIF2α (S-51)
eIF2α
β-tubulin
B
Quantification of p-eIF2α (S-51)
Fold change
p53+/+
p53-/-
siCt
sip53
Ct Dox AZD
C
Torin 1 (100 nM)
AZD8055 (100 nM)
Rapamycin (100 nM)
Time (hours)
3 6 9 16 24
p-eIF2α (S-51)
eIF2α
p-4E-BP1 (S-65)
4EBP1
p-p70 S6K (T-389)
p70 S6K
β-tubulin
D i
A549
Untreated
Doxorubicin
AZD8055
p53
p-p70 S6K (T-389)
p70 S6K
p-4EBP1 (S-65)
4E-BP1
p-eIF2α (S-51)
eIF2α
β-tubulin
D ii
p-p70-S6K (T-389)
Fold change
Ct Dox AZD8055
p-eIF2α (S-51)
Fold change
Ct Dox AZD8055
E i
A549
siCt
sip53
AZD8055
Dox
p53
SESN2
p-p70 S6K (T-389)
p70 S6K
p-4EBP1 (S-65)
4E-BP1
p-eIF2α (S-51)
eIF2α
β-tubulin
E ii
p-p70-S6K (T-389)
Fold change
siCt
sip53
Ct Dox AZD8055
p-eIF2α (S-51)
Fold change
siCt
sip53
Ct Dox AZD8055
F i
BT474
32°c
37°c
AZD8055
Dox
p53
SESN2
p-p70 S6K (T-389)
p70 S6K
p-4EBP1 (S-65)
4E-BP1
p-eIF2α (S-51)
eIF2α
β-tubulin
F ii
p-p70-S6K (T-389)
Fold change
32°c
37°c
Ct Dox AZD8055
p-eIF2α (S-51)
Fold change
32°c
37°c
Ct Dox AZD8055

Figure 3

Figure 3. mTOR inhibition enhanced the phosphorylation of eIF2α through a crosstalk signalling cascade.

A. Wild-type p53 MCF10A cells ($p53^{+/+}$), p53 knockout MCF10A cells ($p53^{-/-}$), and $p53^{+/+}$ cells transfected with either control non-targeting siRNA (siCt) or siRNA specific for p53 (sip53) were treated doxorubicin (500 nM) or AZD8055 (100 nM) for 16 hours. Cells were lysed and analysed by immunoblotting with the indicated antibodies. Blots shown were representative of three independent repeats.

B. Quantification of eIF2α phosphorylation at Ser-51 from blots shown in B. Error bars represent mean ± SD (*n* = 3), ***P* = <0.01, **P* = <0.05, by unpaired student's *t*-test (*ns* = not significant).

C. MCF10A $p53^{+/+}$ cells were treated with mTOR inhibitors: Torin 1 (100 nM), AZD8055 (100 nM) or Rapamycin (100 nM); for the indicated time. Cells were lysed and analysed by immunoblotting with the indicated antibodies.

D. (i) A549 cells were treated with doxorubicin (500 nM) or AZD8055 (100 nM) for 16 hours and analysed by immunoblotting with the indicated antibodies. Blots shown were representative of three independent repeats. (ii) Quantification of p70 S6K phosphorylation at T-389 and eIF2α phosphorylation at Ser-51 from blots shown in (i). Error bars represent mean ± SD (*n* = 3), ****P* = <0.001, ***P* = <0.01, **P* = <0.05, by unpaired student's *t*-test.

E. (i) A549 cells were transfected with either control non-targeting siRNA (siCt) or siRNA specific for p53 (sip53) were treated doxorubicin (500 nM) or AZD8055 (100 nM) for 16 hours. Cells were lysed and analysed by immunoblotting with the indicated antibodies. Blots shown were representative of three independent repeats. (ii) Quantification of p70 S6K phosphorylation at T-389 and eIF2α phosphorylation at Ser-51 from blots shown in (i). Error bars represent mean ± SD (*n* = 3), ****P* = <0.001, **P* = <0.05, by unpaired student's *t*-test (*ns* = not significant).

F. (i) BT474 cells were grown at either 37°c (leading to loss of p53 function) or 32°c (restoring p53 function) and treated doxorubicin (500 nM) or AZD8055 (100 nM) for 16

hours. Cells were lysed and analysed by immunoblotting with the indicated antibodies. Blots shown were representative of two independent repeats. (ii) Quantification of p70 S6K phosphorylation at T-389 and eIF2α phosphorylation at Ser-51 from blots shown in (i). Error bars represent mean $\pm$ SD (n = 2).

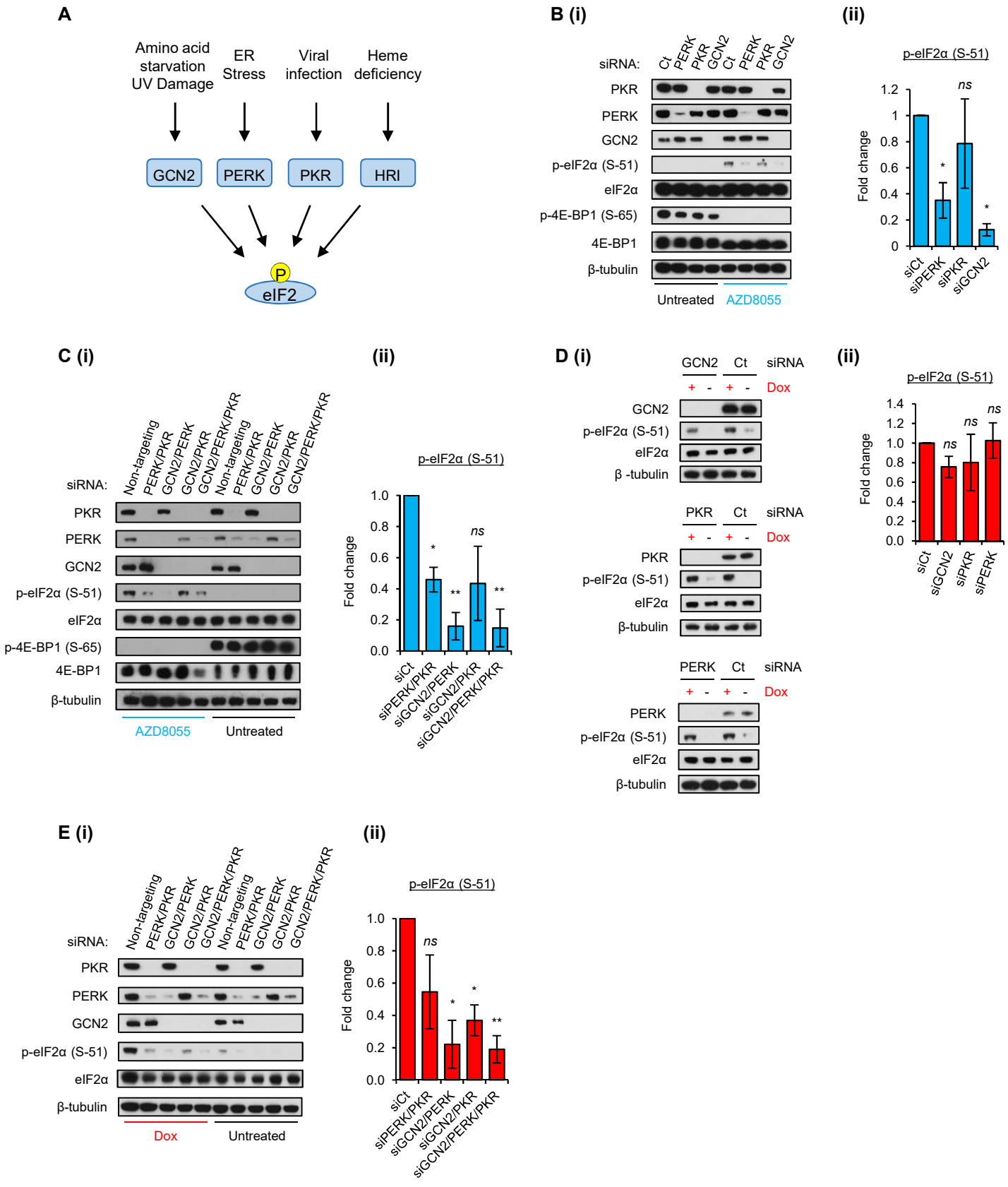
A
Amino acid starvation UV Damage
ER Stress
Viral infection
Heme deficiency
GCN2
PERK
PKR
HRI
P
eIF2
B (i)
siRNA:
Ct
PERK
PKR
GCN2
Ct
PERK
PKR
GCN2
PKR
PERK
GCN2
p-eIF2α (S-51)
eIF2α
p-4E-BP1 (S-65)
4E-BP1
β-tubulin
Untreated
AZD8055
(ii)
p-eIF2α (S-51)
Fold change
ns
siCt
siPERK
siPKR
siGCN2
C (i)
Non-targeting
PERK/PKR
GCN2/PERK
GCN2/PKR
GCN2/PERK/PKR
siRNA:
PKR
PERK
GCN2
p-eIF2α (S-51)
eIF2α
p-4E-BP1 (S-65)
4E-BP1
β-tubulin
AZD8055
Untreated
(ii)
p-eIF2α (S-51)
Fold change
siCt
siPERK/PKR
siGCN2/PERK
siGCN2/PKR
siGCN2/PERK/PKR
D (i)
GCN2
Ct
siRNA
Dox
GCN2
p-eIF2α (S-51)
eIF2α
β -tubulin
PKR
Ct
siRNA
Dox
PKR
p-eIF2α (S-51)
eIF2α
β-tubulin
PERK
Ct
siRNA
Dox
PERK
p-eIF2α (S-51)
eIF2α
β-tubulin
(ii)
p-eIF2α (S-51)
Fold change
siCt
siGCN2
siPKR
siPERK
E (i)
Non-targeting
PERK/PKR
GCN2/PERK
GCN2/PKR
GCN2/PERK/PKR
siRNA:
PKR
PERK
GCN2
p-eIF2α (S-51)
eIF2α
β-tubulin
Dox
Untreated
(ii)
p-eIF2α (S-51)
Fold change
siCt
siPERK/PKR
siGCN2/PERK
siGCN2/PKR
siGCN2/PERK/PKR

Figure 4

Figure 4. Doxorubicin-induced eIF2α phosphorylation was mediated by eIF2Ks GCN2 and PERK

A. Schematic representation of the phosphorylation of eIF2α in response to the activation of eIF2Ks: PERK, GCN2 and PKR, in response to the indicated stimuli.

B. $p53^{+/+}$ MCF10A cells were transfected with individual siRNAs specific toward endogenous eIF2Ks PERK (1 nM), PKR (1 nM) and GCN2 (2 nM). 48-hours post-transfection, cells were treated with AZD8055 (100 nM) for 16 hours. (i) Cells were lysed and analysed by immunoblotting with the indicated antibodies. Blots shown were representative of three independent repeats. (ii) Quantification of eIF2α phosphorylation (ser-51). Error bars represent mean ± SD (*n* = 3), **P* = <0.05, by unpaired student's *t*-test (*ns* = not significant).

C. $p53^{+/+}$ MCF10A cells were transfected with combinations of siRNA specific toward endogenous eIF2Ks PERK (1 nM), PKR (1 nM) and GCN2 (2 nM). 48-hours post-transfection, cells were treated with AZD8055 (100 nM) for 16 hours. (i) Cells were lysed and analysed by immunoblotting with the indicated antibodies. Blots shown were representative of three independent repeats. (ii) Quantification of eIF2α phosphorylation (ser-51). Error bars represent mean ± SD (*n* = 3), **P* = <0.05, ***P* = <0.01, by unpaired student's *t*-test (*ns* = not significant).

D. $p53^{+/+}$ MCF10A cells were transfected with individual siRNAs specific toward endogenous eIF2Ks PERK (1 nM), PKR (1 nM) and GCN2 (2 nM). 48-hours post-transfection, cells were treated with doxorubicin (500 nM) for 16 hours. (i) Cells were lysed and analysed by immunoblotting with the indicated antibodies. Blots shown were representative of three independent repeats. (ii) Quantification of eIF2α phosphorylation (ser-51). Error bars represent mean ± SD (*n* = 3) and significance was calculated by unpaired student's *t*-test (*ns* = not significant).

E. $p53^{+/+}$ MCF10A cells were transfected with combinations of siRNA specific toward endogenous eIF2Ks PERK (1 nM), PKR (1 nM) and GCN2 (2 nM). 48-hours post-transfection, cells were treated with doxorubicin (500 nM) for 16 hours. (i) Cells were lysed and analysed by immunoblotting with the indicated antibodies. Blots shown were representative of three independent repeats. (ii) Quantification of eIF2α phosphorylation (ser-51). Error bars represent mean $\pm$ SD (*n* = 3), **P* = <0.05, ***P* = <0.01, by unpaired student's *t*-test (*ns* = not significant).

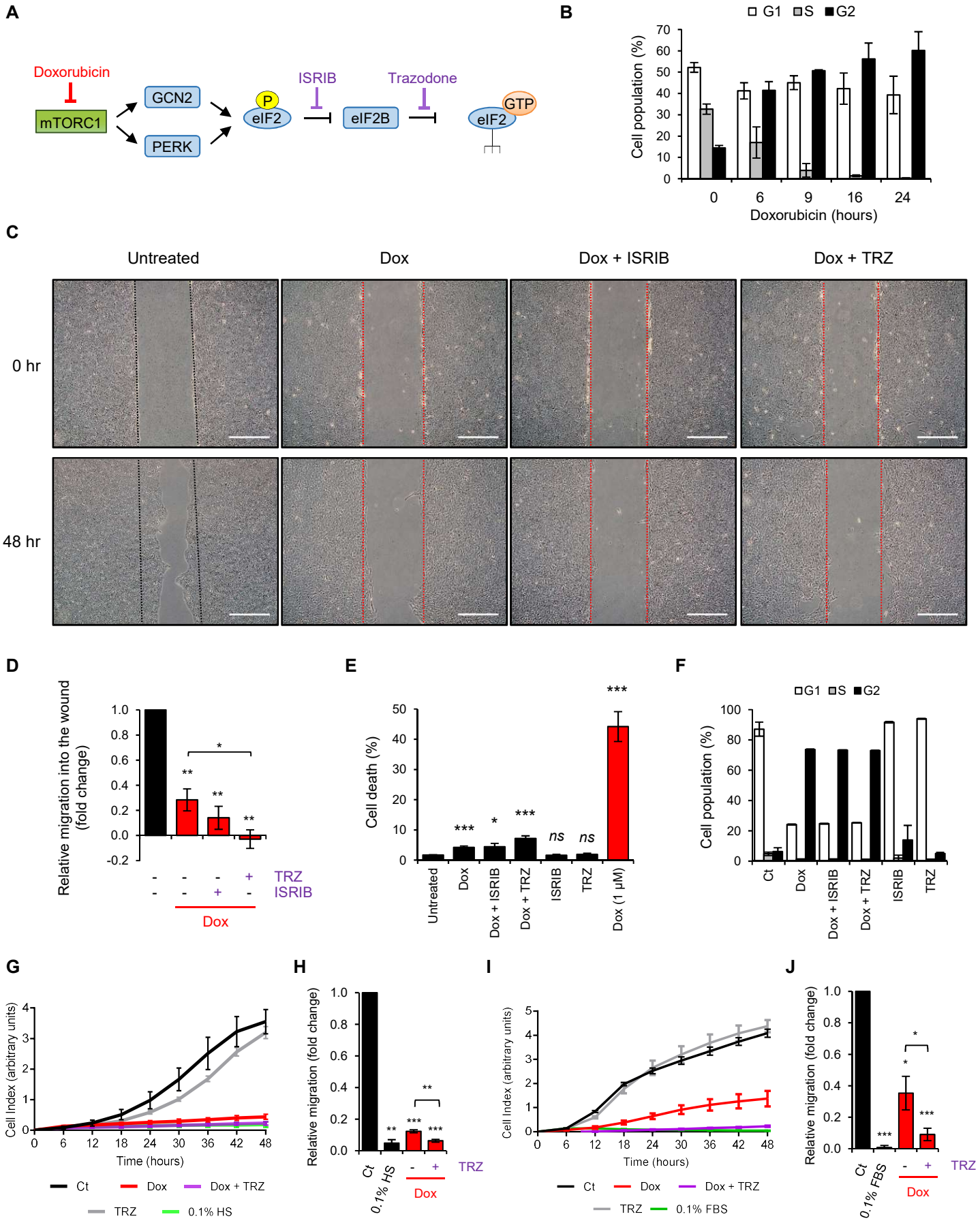
A
Doxorubicin
mTORC1
GCN2
PERK
P
eIF2
ISRIB
eIF2B
Trazodone
GTP
eIF2
B
G1 S G2
Cell population (%)
Doxorubicin (hours)
C
Untreated
Dox
Dox + ISRIB
Dox + TRZ
0 hr
48 hr
D
Relative migration into the wound (fold change)
TRZ
ISRIB
Dox
E
Cell death (%)
Untreated
Dox
Dox + ISRIB
Dox + TRZ
ISRIB
TRZ
Dox (1 μM)
F
G1 S G2
Cell population (%)
Ct
Dox
Dox + ISRIB
Dox + TRZ
ISRIB
TRZ
G
Cell Index (arbitrary units)
Time (hours)
Ct
Dox
Dox + TRZ
TRZ
0.1% HS
H
Relative migration (fold change)
Ct
0.1% HS
TRZ
Dox
I
Cell Index (arbitrary units)
Time (hours)
Ct
Dox
Dox + TRZ
TRZ
0.1% FBS
J
Relative migration (fold change)
Ct
0.1% FBS
TRZ
Dox

Figure 5

Figure 5. Doxorubicin-induced mTOR – eIF2 crosstalk signalling mediates cell migration

A. Schematic representation of mTOR-eIF2 crosstalk signalling and the alleviation of eIF2α phosphorylation-dependent translational repression.
B. Cell cycle analysis of wild-type p53 MCF10A cells ($p53^{+/+}$) treated with doxorubicin (500 nM) for the indicated time period. Cells were incubated with EdU (10 μM) for the final 1.5 hours of treatment (to quantify S-phase cells) and stained with FxCycle violet dye (to quantify cells within G1 and G2 phases) and analysed by flow cytometry. Data values were an average of three independent experiments and error bars represent mean ± SD (*n* = 3).
C. Wound healing assay following treatment with doxorubicin (500 nM), ISRIB (200 nM) or trazodone (50 μM) for 24 hours. The wound was made with a p200 pipette tip (0 hr) and migration into the wound was analysed by microscopy after 48 hours. Dashed lines represent the area of the initial wound and the scale bar represents 500 μM. Images are representative from three independent experiments.
D. Quantification of cell migration into the wounded area from (C) using Image J. All values are displayed relative to the migration of the untreated sample. Error bars represent mean ± SD (*n* = 3), **P* = <0.05, ***P* = <0.01, by unpaired student's *t*-test.
E. Quantification of cell death using Annexin-V-FITC and Draq7 staining of MCF10A $p53^{+/+}$ cells treated with a combination of doxorubicin (500 nM), ISRIB (200 nM) or trazodone (50 μM) for 72 hours. Error bars represent mean ± SD (*n* = 3), ****P* = <0.001, **P* = <0.05, by unpaired student's *t*-test (*ns* = not significant).
F. Quantification of cell cycle state using FxCycle staining in MCF10A $p53^{+/+}$ cells treated with a combination of doxorubicin (500 nM), ISRIB (200 nM) or trazodone (50 μM) for 72 hours. Error bars represent mean ± SD (*n* = 2).
G. Cell migration profiles from xCELLigence RTCA DP instrument. MCF10A cells were treated for 24 hours with doxorubicin (500 nM) or trazodone (50 μM) prior to seeding

in the upper well of the migration CIM-16 plate, and migration was monitored for 48 hours. Media containing only 0.1% horse serum was used as a negative control. Data values were an average of three independent experiments and error bars represent mean ± SD (*n* = 3).

H. Quantification of cell migration relative to the untreated sample from (G) at 48 hours. Error bars represent mean ± SD (*n* = 3), ***P* = <0.01, ****P* = <0.001, by unpaired student's *t*-test.

I. Cell migration profiles from xCELLigence RTCA DP instrument. A549 cells were treated for 24 hours with doxorubicin (500 nM) or trazodone (50 μM) prior to seeding in the upper well of the migration CIM-16 plate, and migration was monitored for 48 hours. Media containing only 0.1% FBS was used as a negative control. Data values were an average of three independent experiments and error bars represent mean ± SD (*n* = 3).

J. Quantification of cell migration relative to the untreated sample from (I) at 48 hours. Error bars represent mean ± SD (*n* = 3), **P* = <0.05, ****P* = <0.001, by unpaired student's *t*-test.

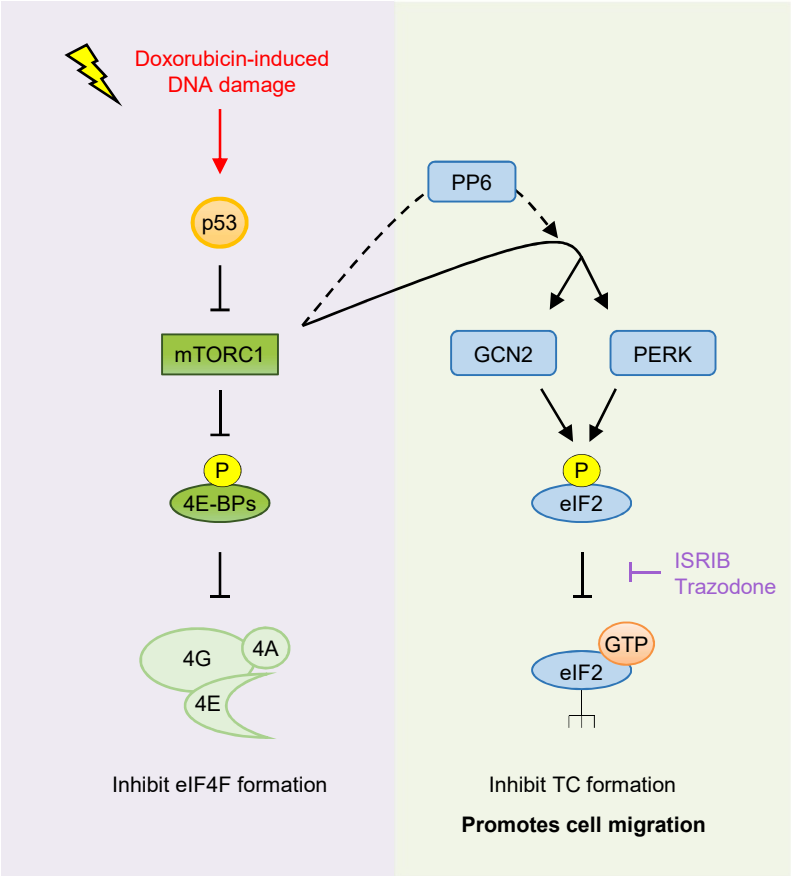
Doxorubicin-induced
DNA damage
p53
mTORC1
P
4E-BPs
4G
4A
4E
Inhibit eIF4F formation
PP6
GCN2
PERK
P
eIF2
ISRIB
Trazodone
GTP
eIF2
Inhibit TC formation
Promotes cell migration

Figure 6

Figure 6. A model of doxorubicin-induced mTOR-eIF2K crosstalk signalling.

Doxorubicin-induced DNA damage leads to the activation of p53 and subsequent inhibition of mTOR via TSC independent mechanisms, most likely resulting in the inhibition of global protein synthesis. Inhibition of mTOR activity directly promotes the activation of both GCN2 and PERK, possibly in a PP6 dependent manner, to enhance the phosphorylation of eIF2α and decrease the availability of ternary complex. Moreover, crosstalk signalling-mediating eIF2α phosphorylation is required for cell migration. Our data suggest that in a tumour setting this signalling pathway could regulate cell adaptation to promote invasion and metastasis.

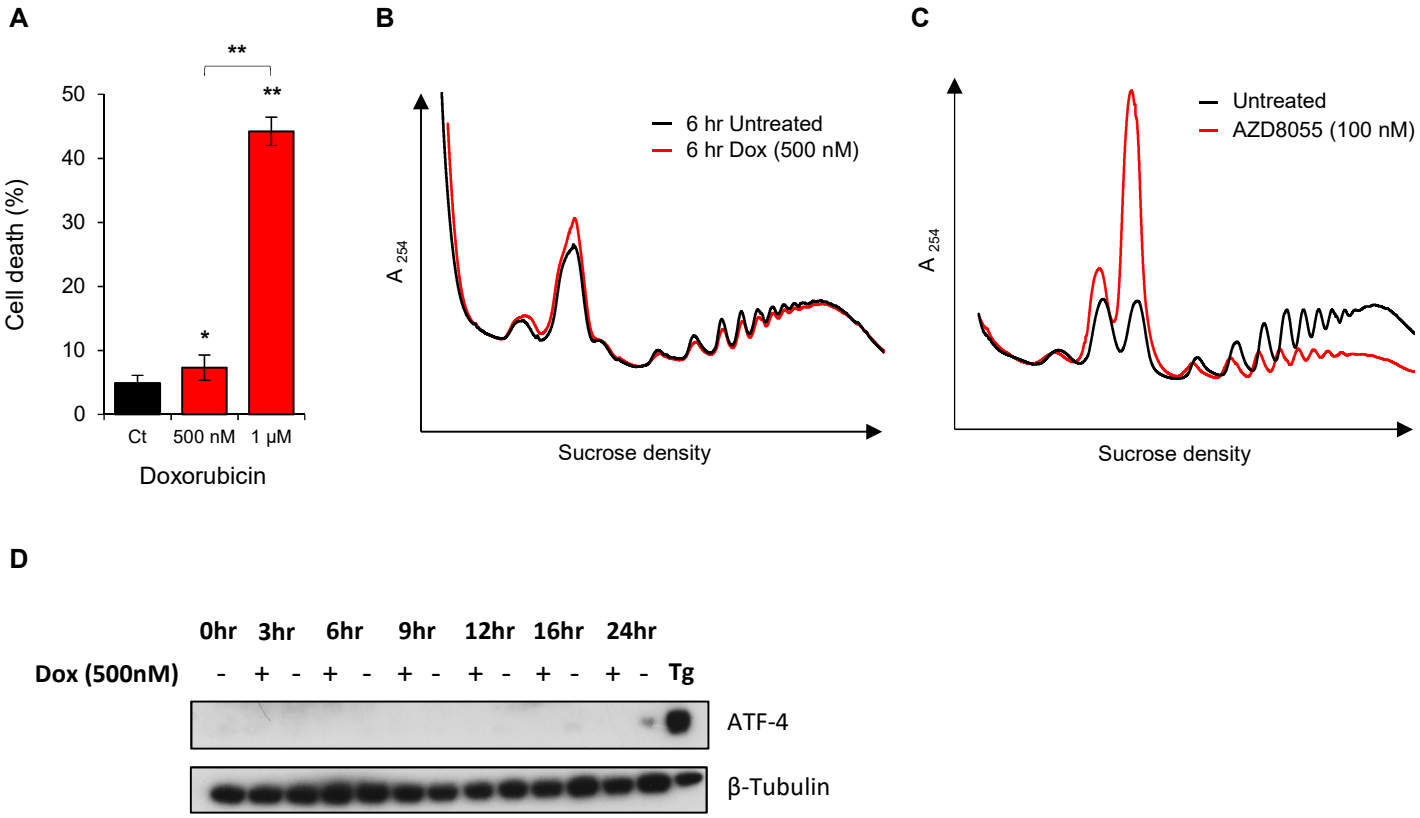

Supplementary Figure 1

Figure S1. Doxorubicin inhibited protein synthesis and induced cell death In MCF10A cells.

A. Quantification of cell death using Annexin-V-FITC and Draq7 staining in wild-type p53 MCF10A cells ($p53^{+/+}$) treated with doxorubicin (500 nM or 1 μM) for 24-hours. Error bars represent mean ± SD (*n* = 3), ***P* = <0.01, **P* = <0.05, by unpaired student's *t*-test.

B. Comparison of polysome profiles from MCF10A $p53^{+/+}$ cells untreated or treated continuously with doxorubicin (500 nM) for 6 hours. Cytoplasmic lysates were centrifuged at 38000 rpm through 10%-50% sucrose gradients at 4°C for two hours, and absorbance was measured at 254 nm using a flow rate of 1 ml/min.

C. Comparison of polysome profiles from MCF10A $p53^{+/+}$cells untreated or treated continuously with catalytic mTOR inhibitor AZD8055 (100 nM) for 3 hours. Cytoplasmic lysates were centrifuged at 38000 rpm through 10%-50% sucrose gradients at 4°C for two hours, and absorbance was measured at 254 nm using a flow rate of 1 ml/min.

D. ATF4 expression was monitored in MCF10A cells treated with doxorubicin (500 nM) for the indicated time by immunoblotting. Thapsigargin (1 μM for 1 hour) was used as a positive control to upregulate ATF4 expression. Blots shown were representative of three independent repeats.

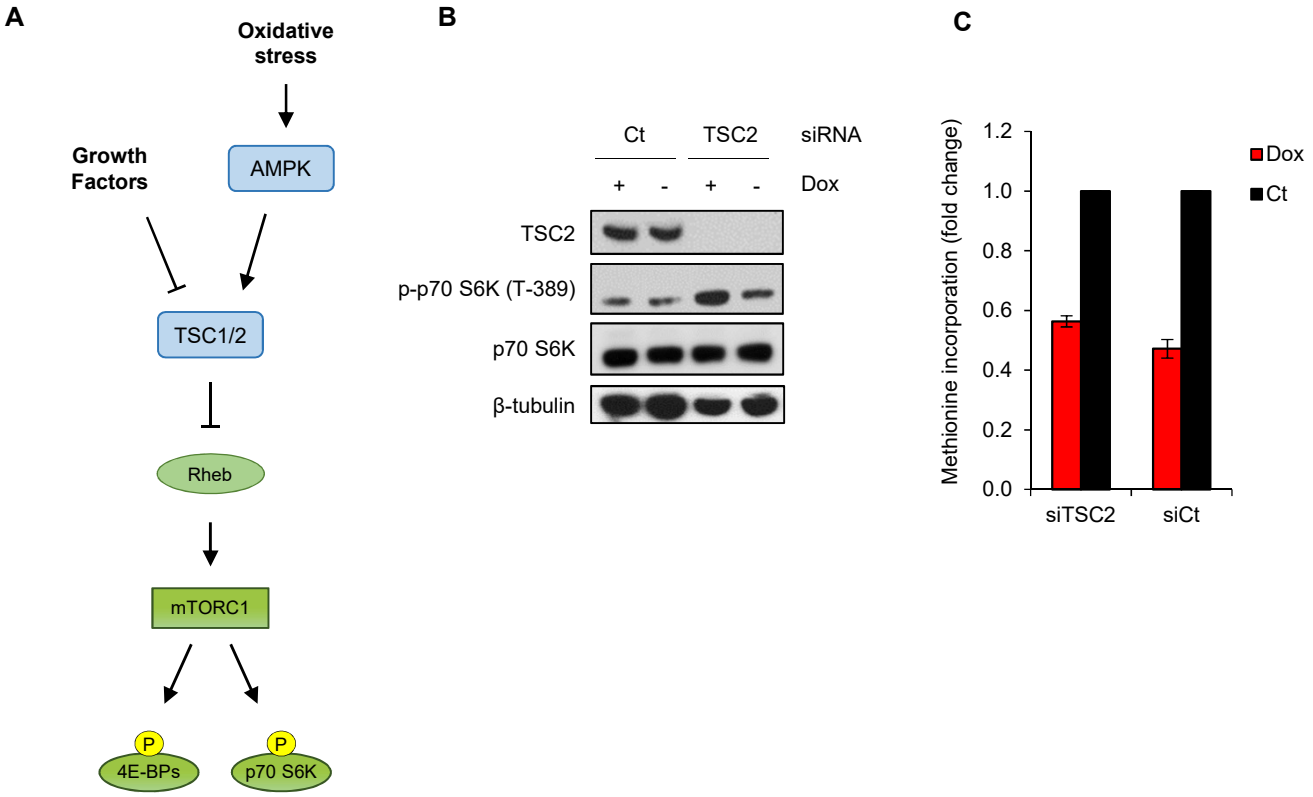

Supplementary Figure 2

Figure S2. Doxorubicin-induced mTORC1 inhibition was not dependent on TSC activity.

A. Schematic representation of the regulation of Tuberous sclerosis complex (TSC) and its subsequent regulation of mTORC1 activity.

B. $p53^{+/+}$ MCF10A cells were transfected with siRNA specific toward TSC2 (1 nM) to downregulate TSC1/2 activity. 48-hours post-transfection, cells were treated with doxorubicin (500 nM) for 24 hours, lysed and analysed by immunoblotting with the indicated antibodies. Blots shown were representative of two independent repeats.

C. $p53^{+/+}$ MCF10A cells were transfected with siRNA specific toward TSC2 (1 nM) to downregulate TSC1/2 activity. 48-hours post-transfection, cells were treated with doxorubicin (500 nM) for 24 hours and pulse-labelled with $^{[35]}$S-methionine for 30 minutes. Total counts per minute were normalised to total protein. Error bars represent mean $\pm$ SD (n = 2).

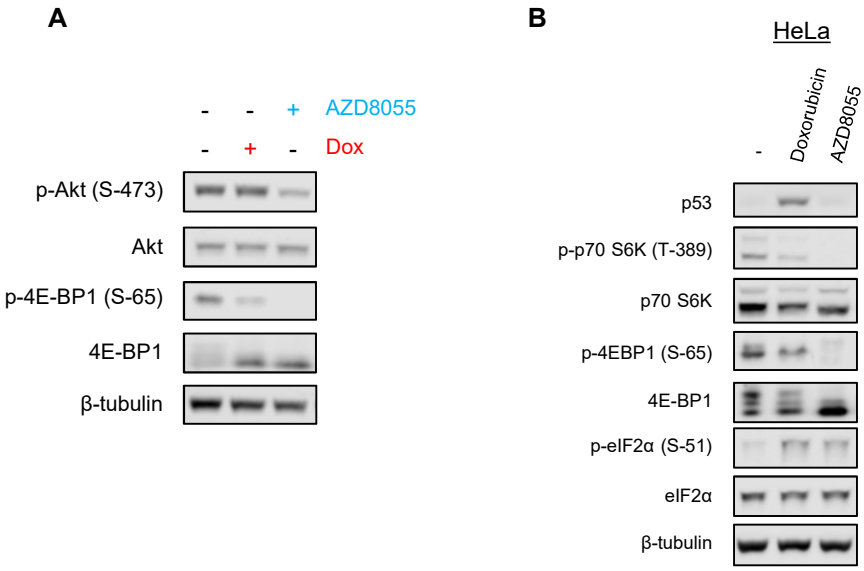

Supplementary Figure 3

Figure S3. Doxorubicin inhibits mTORC1 signalling

A. MCF10A cells were treated with doxorubicin (500 nM) or AZD8055 (100 nM) for 16 hours and analysed by immunoblotting with the indicated antibodies. Blots shown were representative of three independent repeats.
B. HeLa cells were treated with doxorubicin (500 nM) or AZD8055 (100 nM) for 16 hours and analysed by immunoblotting with the indicated antibodies.

A

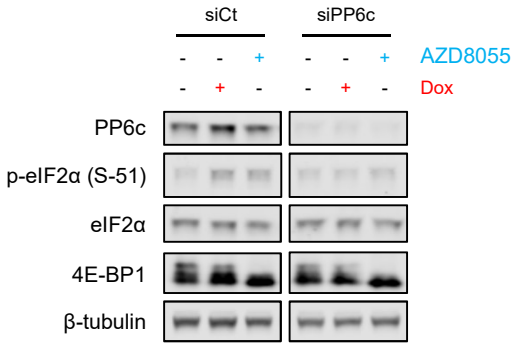

B

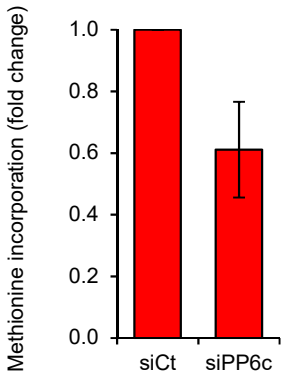

Supplementary Figure 1

Figure S4. Knockdown of PP6 activity reduced protein synthesis rates

A. $p53^{+/+}$ MCF10A cells were transfected with an siRNA specific for PP6c and treated with doxorubicin (500 nM) or AZD8055 (100 nM) for 16 hours. Cells were lysed and analysed by immunoblotting with the indicated antibodies. Blots shown were representative of three independent repeats.

B. $p53^{+/+}$ MCF10A cells were transfected with an siRNA specific for PP6c for 48 hours and pulse-labelled with $^{[35]}$S-methionine for 30 minutes. Total counts per minute were normalised to total protein and values are shown as a fold change relative to non-targeting siRNA (siCt). Error bars represent mean ± SD (*n* = 3).

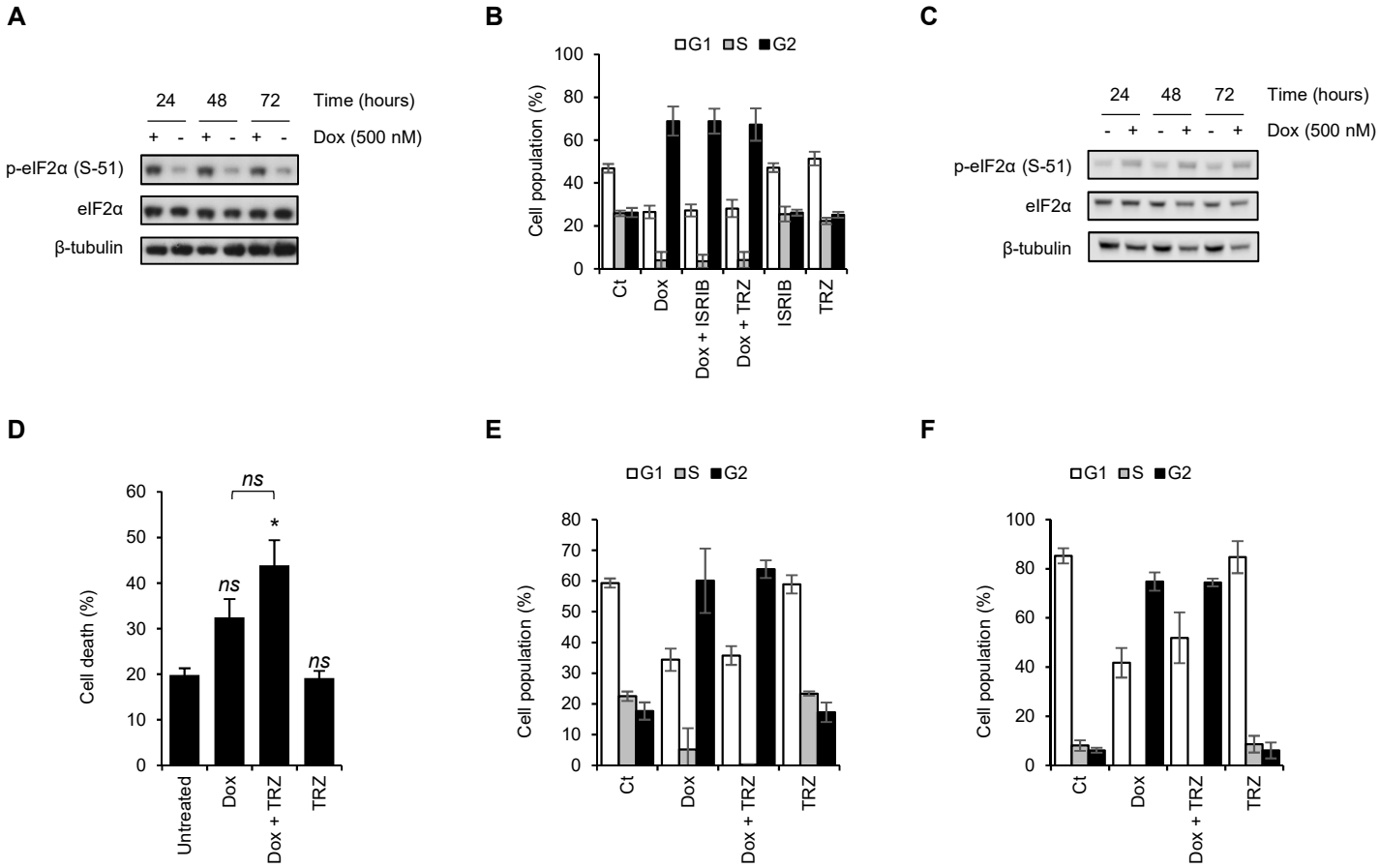

Supplementary Figure 5

Figure S5. eIF2α-mediated cell migration was not caused by changes in cell death or cell cycle regulation

A. MCF10A $p53^{+/+}$ cells were treated with doxorubicin (500 nM) for the indicated time points and eIF2α phosphorylation was monitored by immunoblotting.

B. Quantification of cell cycle state using FxCycle staining in MCF10A $p53^{+/+}$ cells treated with a combination of doxorubicin (500 nM), ISRIB (200 nM) or trazodone (50 μM) for 24 hours. Error bars represent mean ± SD (*n* = 3).

C. A549 cells were treated with doxorubicin (500 nM) for the indicated time points and eIF2α phosphorylation was monitored by immunoblotting.

D. Quantification of cell death using Annexin-V-FITC and Draq7 staining of A549 cells treated with a combination of doxorubicin (500 nM), ISRIB (200 nM) or trazodone (50 μM) for 72 hours. Error bars represent mean ± SD (*n* = 3), **P* = <0.05, by unpaired student's *t*-test (*ns* = not significant).

E. Quantification of cell cycle state using FxCycle staining in A549 cells treated with a combination of doxorubicin (500 nM), ISRIB (200 nM) or trazodone (50 μM) for 24 hours. Error bars represent mean ± SD (*n* = 3).

F. Quantification of cell cycle state using FxCycle staining in A549 cells treated with a combination of doxorubicin (500 nM), ISRIB (200 nM) or trazodone (50 μM) for 72 hours. Error bars represent mean ± SD (*n* = 2).